POLITECNICO
MILANO 1863

SCUOLA DI INGEGNERIA INDUSTRIALE
E DELL'INFORMAZIONE

Theoretical study of high-power laser interaction with novel nano-structured foam materials for inertial confinement fusion research

Tesi di Laurea Magistrale in
Nuclear Engineering - Ingegneria Nucleare

Author: **Vittorio Ciardiello**

Student ID: 941603
Advisor: Prof. Matteo Passoni
Co-advisors: Alessandro Maffini, Arianna Formenti, Fabrizio Consoli, Mattia Cipriani
Academic Year: 2021-22

Abstract

This thesis regards the work done in collaboration with the Centro Ricerche ENEA (Frascati) with the aim to analyze novel materials for Inertial Confinement Fusion (ICF) applications. ICF is the branch of fusion research devoted to understand if nuclear fusion can be successfully achieved for commercial purposes by irradiating with High Intensity Lasers (HIL) a fuel pellet, a layered sphere of a few mm of diameter. These novel materials are known as foams. The foams I considered are those produced by the Politecnico di Milano at the NanoLab group by the Pulsed Laser Deposition (PLD) technique. The foams realized by this technique exhibit a nanostructure and so they are said to be nanostructured materials. There a number of articles devoted to the applications of these specific foams outside the fusion research, such as particle's acceleration and generation [19, 20, 24, 26, 27]. One of the aims of my thesis more specifically is to understand if this technique can be used for producing two of the main components of an ICF apparatus: the ablator and the hohlraum. ICF can be carried out by means of different approaches. The main ones are known as direct drive and indirect drive. In the former the HIL directly irradiates the target, in the latter the fuel pellet is placed into a cylindrical chamber called hohlraum; the HIL irradiates the hohlraum's walls and the X-rays are produced have to irradiate the ablator. These schemes have of course advantages and disadvantages, as I am going to show later in the thesis development. The ablator is the most external layer of the fuel pellet whose aim, in the direct drive approach, is to convert as much laser energy as possible into energy available for igniting the fuel at the fuel pellet's core (also called hot spot). Foams produced by the PLD have the potentialities for producing both better ablators and hohlraums. For what concerns the former the use of foams lead to much higher pressure levels and efficiency of absorptions [8, 11]. For what concerns the latter Low Density Gold (LDG) targets exhibit higher conversion efficiencies of the laser energy into X-rays [32]. My work consisted in performing simulations with the hydrodynamic code (MULTI-FM 1D) for understanding the features of the irradiation of these foams and then for designing targets to be used in experiments at the ABC facility which is the laser facility available at the Centro Ricerche ENEA. For both these applications I got novel results. I have shown that foams made with carbon are potentially better

ablators than their bulk counterpart. On the other hand I have shown that foams made with gold are for sure of interest for making hohlraums since my simulations shown an higher convertion efficiency of the laser energy into X-rays. This work once validated by experiments will represents a starting point for designing new ICF components.

Keywords: Laser,nanostructured materials, ENEA, ABC,Politecnico di Milano

Abstract in lingua italiana

Questo lavoro di tesi è stato svolto in collaborazione con il Centro Ricerche ENEA (Frascati) con l'obiettivo di analizzare materiali innovativi per applicazioni di Inertial Confinement Fusion (ICF). La ICF è la branca della ricerca sulla fusione dedicata a capire se la fusione nucleare può essere ottenuta con successo per scopi commerciali irradiando con High Intensity Lasers (HIL) un pellet di combustibile, una sfera stratificata di pochi mm di diametro. Questi nuovi materiali sono conosciuti come foams. Le foams che ho considerato sono quelle prodotte dal Politecnico di Milano presso il gruppo NanoLab con la tecnica della Pulsed Laser Deposition (PLD). Le foams realizzate con questa tecnica presentano una nanostruttura e quindi ricadono nella definizione di materiali nanostrutturati. Esistono numerosi articoli dedicati alle applicazioni delle foams al di fuori della ricerca sulla fusione, come l'accelerazione e la generazione di particelle [19, 20, 24, 26, 27]. Uno degli obiettivi della mia tesi più nello specifico è capire se questa tecnica può essere utilizzata per produrre due dei componenti principali di un apparato ICF: l'ablatore e l'hohlraum. L'ICF può essere effettuato con diversi approcci. I principali sono conosciuti come direct driven e indirect driven. Nel primo l'HIL irradia direttamente il bersaglio, nel secondo il pellet di combustibile è posto in una camera cilindrica chiamata hohlraum; l'HIL irradia le pareti dell'hohlraum e i raggi X prodotti devono irradiare l'ablatore. Questi schemi hanno ovviamente vantaggi e svantaggi, come mostrerò più avanti nello sviluppo della tesi. L'ablatore è lo strato più esterno del pellet di carburante il cui scopo, nell'approccio ad azionamento diretto, è convertire quanta più energia laser possibile in energia disponibile per accendere il carburante nel nucleo del pellet di carburante (chiamato anche hot spot). Le foams prodotte dal PLD hanno le potenzialità per produrre sia migliori ablatori che hohlraum. Per quanto riguarda i primi l'uso di schiume porta a livelli di pressione ed efficienza degli assorbimenti molto più elevati [8, 11]. Per quanto riguarda l'hohlraum è stato dimostrato che bersagli Low Density Gold (LDG) esibiscono una maggiore efficienza di conversione dell'energia laser in raggi X [32]. Il mio lavoro è consistito nell'eseguire simulazioni con il codice idrodinamico (MULTI-FM 1D) per comprendere le caratteristiche dell'irraggiamento di queste foams e quindi per progettare bersagli da utilizzare negli esperimenti presso l'impianto ABC che è l'impianto laser disponibile presso

il Centro Ricerche ENEA. Per entrambe queste applicazioni ho ottenuto nuovi risultati. Ho dimostrato che le foams realizzate con il carbonio sono potenzialmente migliori ablatori rispetto alla loro controparte a densità standard. D'altra parte ho dimostrato che le foams fatte con l'oro sono di sicuro interesse per la realizzazione di hohlraum poiché le mie simulazioni hanno mostrato una maggiore efficienza di conversione dell'energia laser in raggi X. Questo lavoro, una volta convalidato dagli esperimenti, potrà rappresentare un punto di partenza per la progettazione di nuovi componenti ICF.

Parole chiave: Laser,materiale nanostrutturato,Politecnico di Milano, NanoLab,ENEA,ABC

Contents

1 | Introduction to Inertial Confinement Fusion

1.1. An overview about Nuclear fusion

Nuclear fusion is the most promising way to produce green energy in the next future. Nowadays there are a number of technical issues which must be resolved. There are no nuclear fusion reactors able to be used for commercial distribution. On the other hand there are many experimental reactors which are able to sustain, for a short time, the conditions required for nuclear fusions taking place in a controlled environment. Worldwide a lot of efforts are continuosly made to achieve suitable conditions for fusion with a Deterium-Tritium mixture, which has a high release of energy as alpha particles and neutrons, and a favorable cross section at energies reachable in a laboratory. There are two main strategies to approach the nuclear fusion problem; Magnetic Confinement Fusion (MCF) and Inertial Confinement Fusion (ICF). In the former an hot and rarefied plasma needs to be confined for a relatively long time by using strong magnetic fields in machines known as "Tokamak", in the latter a small fuel pellet needs to be ablated by High Intensity Lasers (HIL). Both these strategies have shown important results. In the 2021 the National Ignition Facility (NIF) in Livermore established the record of energy yield from fusion reactions demonstrating that the breakeven is possible. For what concerns the Magnetic Confinement Fusion in the beginning of 2022 the chinese reactor EAST has been able to operate for about 100 seconds. Despite the great importance of these results, the production of electric energy through nuclear fusion is still a long way off. In Europe we have many important facilities. In Cadarache the machine ITER, which is the biggest experimental Tokamak ever build in Europe, is about to be completed. It is composed by magnetic superconductive coils whose dimensions are 20 meters in height and 10 meters in width. The criogenic system required to make them work properly is bigger than the one already operating for the LHC in CERN. In Bourdeaux we have Laser Mega Joule, which is nanosecond laser with an energy per pulse of about 1 MJ. In Italy the largest laser in terms of energy per pulse (100 J) is the ABC facility in Centro Ricerche ENEA

in Frascati. In ICF, which is the focus of this thesis work, the confinement time is as small as the time needed for a fuel pellet to be destroyed once irradiated by high intensity lasers. As defined by the Lawson's criterion, the product among density, temperature and energy confinement time must be not smaller than a quantity defined by the mixture characteristics and the ignition strategy. Let us start with MCF [36]:

$$n\tau_E T \simeq 3.3 \times 10^{15} \mathrm{cm}^{-3} \mathrm{sKeV}. \tag{1.1}$$

where:

- n is the particle density as particles/cm^{-3};
- τ_E energy confinement time in seconds;
- T is the fuel temperature in KeV;

In order to define an analogous criterion in the ICF case I need to define first what is the hot spot. The hot spot is the most internal region of the fuel pellet. In this region, thanks to an enourmous supplying of energy, nuclear fusions can occur. So in the hot spot we immagine that the conditions for the Lawson criterion can be achieved [36].

$$\rho_h R_h T_h > 6 \left(\frac{\rho_h}{\rho_c} \right)^{0.5} \tag{1.2}$$

where:

- ρ_h is the fuel mass density of the hot spot in $\frac{\mathrm{g}}{\mathrm{cm}^3}$;
- R_h is the hot spot radius in cm;
- T_h is the fuel temperature into the hot spot in KeV;
- ρ_c is the fuel mass density in the cold region sorrounding the hot spot

In nature nuclear fusion occurs continuosly in the stars. In that case all the particles are confined by gravity. The quantities to look at in order to understand if nuclear fusions can take place are density, confinement time and temperature. In the core of a star these quantities are high. The temperature is in the order of tens million celsius degrees, density in the order of thousands of the solid state and confinement time in the order of the time required for a charged particle to escape the core region. The core has a radius of about 0.2 solar radii. A proton at 100 million celsius degrees has a velocity of about 100 million m/s (in this rough estimate I am not considering relativistic effects), therefore if it could move along a straight line starting from the center the confinement time would be a matter

of seconds. This is of course a lower limit. On Earth we are not able to build a similar machine. We have to make a choice on which are the parameters we want to take as high and which are those we take as low. The temperature must be high since it's directly involved into the cross section of the process. So the confinement time and the density have to be properly adapted. One of the approaches developed in order to reproduce what happens in the stars is the so called Inertial Confinement Fusion (ICF). In this approach we have a closed chamber into which a fuel pellet is placed. A set of High Intensity Lasers (HIL) is used to ablate the pellet. The locution inertial confinement comes from the fact that in this approach the confinement time of the fuel is entirely up to the mass inertia of the fuel itself. So considering that the fuel pellet is a sphere whose diameter is few mm the confinement time is a matter of nano-seconds. So in this approach we must achieve very high temperature and density of the fuel since the confimenet time is so small. More precisely the fuel pellet is a layered sphere. All the layers have a precise purpose. The most external one is called ablator. The role of the ablator is to absorb as much laser energy as possible, converting it into thermal and kinetic energy transported by the shock waves and radiation generated by the interaction with the laser. These shock waves must be able to transport energy through the pellet reaching the most internal region into which the Lawson criterion must be satisfied (hot spot). An asymmetric compression is detrimental for the performances of the capsule. Therefore the ablator must be able to also smooth the irregularities of the absorbed laser energy distribution. The realization of a reliable and efficient ablator is one of the main technical problems to be solved in ICF and in fact this will be one of the problems I will approach in my work.

Compression of the fuel has to be achieved isotropically and isoentropically. The discussion below is partially taken by [36]. The first law of thermodynamics states the energy conservation which can be expressed as $de = Tds + p|dV|$, the specific internal energy of an infinitesimal amount of matter increases by an amount de either due to heat exchange $dq = Tds$, implying an increase of specific entropy ds, or by doing work $-pdV$, where p is the pressure and $V = \frac{1}{\rho}$ the specific volume. An isoentropic compression implies ds=0, which means that the required energy for achiving a given pressure is lower. On the other hand in ICF, since the confinement time is a matter of ns, we need a very fast compression and the dynamic enstablished by a high-power laser beam pulses as considered here leads to strong shock waves, producing unavoidably a large amount of entropy. Mass, momentum, and energy obey to proper conservation laws across a shock. This does not happen for the entropy. By quoting the book of Drake [2] the change of entropy across the shock wave is given by:

$$\begin{cases} s_2 - s_1 = c_v log[\frac{P_2}{P_1}(\frac{\rho_1}{\rho_2})^{\gamma}] \end{cases} \tag{1.3a}$$

- s_1,P_1, ρ_1 are respectively the upstream values of entropy, pressure and density;
- s_2,P_2, ρ_2 are respectively the downstream values of entropy, pressure and density;
- γ is the polytropic index of the ideal gas model;
- c_v is the specific heat at constant volume.

The Hugoniot's equations (Appendix A.1) are consistent with shock waves whose thickness is ideally zero. In reality that thickness is not zero and into the shock front kinetic energy is converted into heat, therefore entropy is generated. We want to keep this entropy generation as low as possible. In order to achieve this goal a multiple shock scheme can be used [2]:

$$\begin{cases} s_{fin} - s_{in} = c_v log\left[\frac{P_{fin}}{P_{in}}(\frac{\rho_{in}}{\rho_{fin}})^{n\gamma}\right] \end{cases} \tag{1.4a}$$

As you can see from the equation above once the limit $n \to +\infty$ is assumed the compression is adiabatic, so no entropy is produced. This phenomenon is a very important one for designing an ignition scheme.
The implosion of the fuel pellet have to take place maximing the pressure while minimizing the entropy production. From this point of view, as reported in Ref. [36], the implosion of hollow spherical shells whose thickness is much smaller than the initial outer radius performs better than the full sphere implosion. The most diffused fuel pellet design uses a cryogenic fuel layer with an initial aspect ratio (which is the ratio of the outer radius of the pellet to the ablator thickness) of about 10 and an outer radius of fews mm (this value results from a design based on a specific class of material, usually plastic ablators). Pressures of the order of 100 Mbar are necessary to cause the shells to implode to a velocity of the order of hundreds of m/s (these numbers have to be seen just as a reference for the typical order of magnitudes involved in this phenomenon). Nowadays the most promising fuel mixture is the Deterium-Tritium, as shown in the following figure:

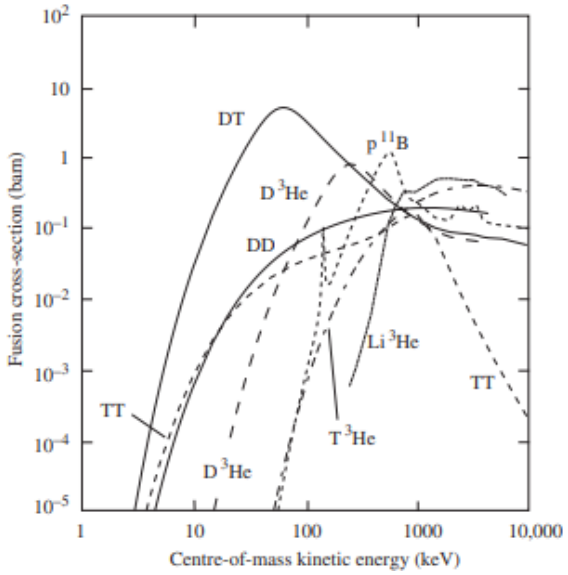

Figure 1.1: The cross-sections of the main fusion reactions as functions of the center of mass kinetic energy [36].

The aforementioned mixture in fact exhibits less severe conditions for reaching the ignition. On the other hand one of the main technological issues related to this mixture is due to the production of high energy neutrons. For this reason other possibilities are under investigation. From this point of view it is worth to mention the proton-boron reaction. This reaction, as shown above, exhibits always a significantly lower cross section with respect to the DT reaction at all temperatures. Despite this great disadvantage this reaction is the only known fusion reaction, at least among those which may be reproduced on Earth, completely neutron free:

$$D + T \rightarrow {}^{4}_{2}\mathrm{He}(3,5MeV) + n(14,1MeV) \tag{1.5a}$$

$$p + {}^{11}_{5}\mathrm{B} \rightarrow 3{}^{4}_{2}\mathrm{He}(8,7MeV) \tag{1.5b}$$

The problem related to the emission of high energy neutrons is twofold. First of all is a matter of material embrittlement since these neutrons are able to induce heavy atomic displacements into the crystalline lattice of structural materials and also nuclear reactions which may lead to the production of intra-lattice gases like helium(whose accumulation destroys the material from inside). Secondly the nuclear reactions induced by neutrons are not just those related to the helium production but also those related to the material radiative activation. Material activation is something very deleterious for the safety of the nuclear plant and leads to very high disposal cost. These problems are so important

that the scientific community is seriously taking into consideration the p-boron mixture even if is much harder to ignite respect to the D-T one.

1.2. Inertial Confinement Fusion (ICF)

In ICF the main technical issues that need to be overcome are related to two main aspects. First the pellet design, which is the main focus of this thesis. Second, the temporal and spatial homogeneity of the laser beams.

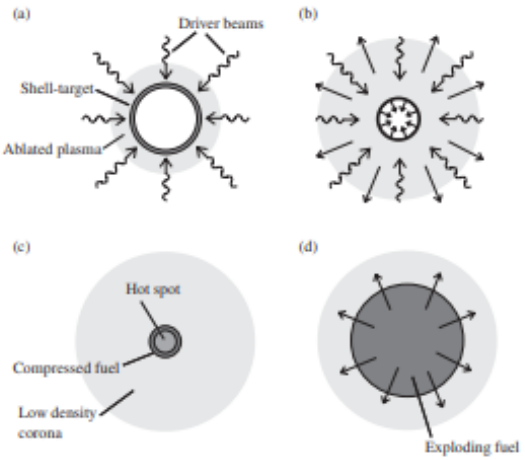

Figure 1.2: Schematic representation of the fuel pellet implosion [36].

The physics of how the ablation, induced by a High Intensity Laser, of the pellet surface can lead to a compression of the pellet itself is related to the momentum balance. The radiation pressure exerted by the laser represents a very small contribution. Once the laser interacts with the most external layer of the pellet, the so called ablator, its mass is ejected toward the laser. Due to the third law of Newton a compression of the internal layers of the pellet is realized.
The design of an optimized ablator will be one of the aim of this thesis work. In the next section different ignition schemes will be presented. The main two approaches to inertial confinement fusion are called Direct Drive and Indirect Drive. In the direct drive the ablator is directly ablated by the high intensity lasers. In the indirect drive the ablator is ablated by X-Rays coming from the so called hohlraum. The hohlraum is a chamber made of high-Z material (gold most of the times) whose role is to convert the laser energy into X-Rays. The reason for this possible configuration will be explained in the next section. For now I will limit myself saying that the design of the hohlraum is another imporant aspect which will be considered in this thesis.

1.3. Direct, indirect drive and non conventional ignition schemes

As anticipated in the previous section there are several possible apporaches under investigation for achieving the conditions for the ignition. Direct and indirect drive are the main configurations, the other which will be presented can be seen as upgrades of them:

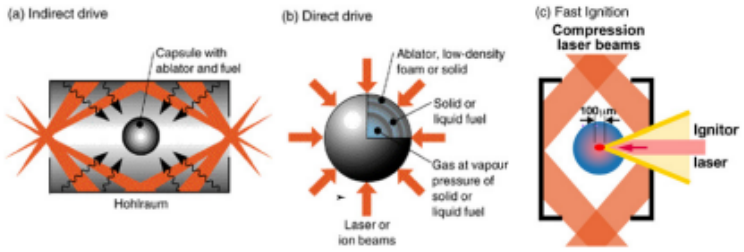

Figure 1.3: Here are represented the main ignition configurations [14].

In this sections I am going to show the main ignition configurations explaining the ideas behind them without entering deeply into details. The aim is to give these basic but mandatory concepts in the most simple way.

1.3.1. Indirect drive

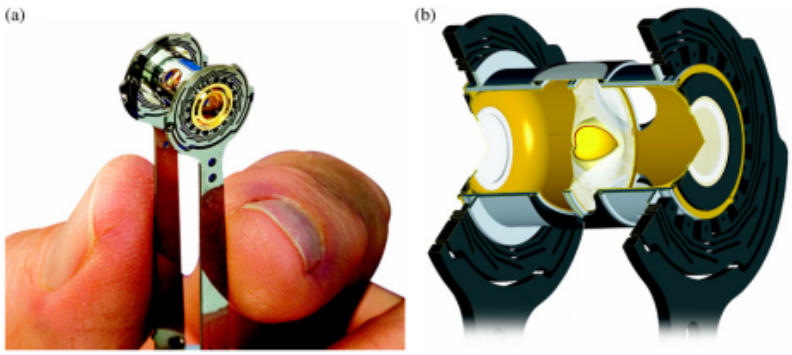

Figure 1.4: This is how a hohlraum looks like [14].

In the indirect-drive configuration the fusion capsule, is keyed inside a cylindrical hohlraum. Laser beams, which enter the through holes which are on both ends of the hohlraum, are absorbed by the internal wall and converted into X-rays. These X-rays fill the hohlraum generating an isotropic photon spectrum and ablate the outer layer of the fuel pellet.This ablation process leads to a compression of fuel, which bring the system to a thermody-

namic state which causes the hot spot to start the ignition; nuclear fusions begin to take place. The conversion of the laser light into X-rays comes at cost, reducing the overall efficiency of conversion of the laser into mechanical energy available for compression. On the other hand in indirect drive, thanks to the X-rays spectrum which obeys to the law of black body radiation (so an isotropic Planckian profile) , issues concerning implosion symmetry and stability are much less severe (but not completely eliminated).
A last comment about indirect drive. To maximize the implosion efficiency an ablator must be a low-Z material such as plastic, carbon. If the ablator would be a high-Z material two important problems would take place. First of all, there would a self generated photon field which would deplete the mechanical energy available for the shock formation (so, conversion efficiency of laser energy to mechanical energy would decrease). Second, the self generated photon field would exhibits a wavelength (X-ray spectrum) which would allow these photons to see the remaining part of the fuel pellet as subcritical and this would lead to a fuel preheat before the compression. By recalling what is written in section 1.1 about entropy generation we can understand that this fuel preheat would be deleterial for the efficiency of compression due to the entropy generation. The symmetry of the compression is one of the biggest problems since a an asymmetric compression leads to lower final pressure so it makes more difficult the achievement of the Lawson criterion into the hot spot.

1.3.2. Direct drive and Shock Ignition

In direct drive, the shock wave is generated by the direct ablation of the outer surface of the fuel pellet by the high intensity lasers. This shock is the responsible for the high pressure levels which are observed at the boundary between the inner surface of the ablator and the outer surface of the second layer of the fuel pellet. In this configuration the efficiency of conversion of the laser energy energy into mechanical energy available for the compression is related only to the ablator performances. It can be shown that the pressure achieved into the hot spot, P_{hs}, must exceed [15] a threshold value P_{th} for the ignition:

$$P_{hs} > P_{th} = 250\text{Gbar}\left(\frac{E_{hs}}{10\text{kJ}}\right)^{-1/2} \tag{1.6}$$

where E_{hs} is the driver energy that is delivered to the hot spot. By increasign E_{hs}, the required pressure and thus fuel convergence for ignition is reduced. The shock ignition design is a modifation of the direct drive one. The stages of compression and hot spot formation are partly separated. The fuel is first compressed at a velocity that is lower than what it would be in conventional ICF. Close to stagnation (a phase of the implosion

at which the product between density and pellet outer radius reaches a critical value), an intense laser pulse is injected driving a strong shock, which allows the hot spot formation [31]. The current shock ignition design was shown by Betti and co-workers in 2007 [6]. The basic idea behind this design was proposed by Shcherbakov in 1983 [37]. The separation of the compression stage from the hot spot formation is way better in than in conventional direct drive scheme. Thanks to the lower implosion velocity there is a lower entropy generation, which is a great advantage since as explained above the entropy generation must be reduced in order to maximize the efficiency of laser to mechanical energy conversion. Moreover, lower laser intensities suppress that issues related to possible parametric instabilities and electronic preheat.

Let me summarize advantages and disadvantages for both these main schemes, namely, direct and indirect drive. For what concerns the former we have simpler targets and overall greater efficiency. The issues are mainly due to an higher sensitivity to electron preheating and to the so called hydrodynamical instabilities which are caused by the anisotropy of the compression stage. On the other hand, in the indirect scheme the symmetrization associated to the X-ray spectrum is able to remove the aforementioned issues. Nevertheless other issues becomes relevant: an efficiency for the X-ray losses through the wall must be taken into account and an higher sensitivity to parametric instabilities such as the stimulated Raman and Brillouin scattering takes place. These parametric instabilities once activated lead unavoidably to lower conversion efficiency since a photon can udergo these phenomena (which are basically scattering phenomena) instead of being absorbed by the ablator.

1.3.3. Fast Ignition

Laser driven fast ignition involves high-current relativistic electron beams and so huge (up to giga-gauss) magnetic fields.The concept of fast ignition of inertial fusion targets is to separate fuel compression from fuel ignition and to ignite pre-compressed fuel by a separate external trigger.

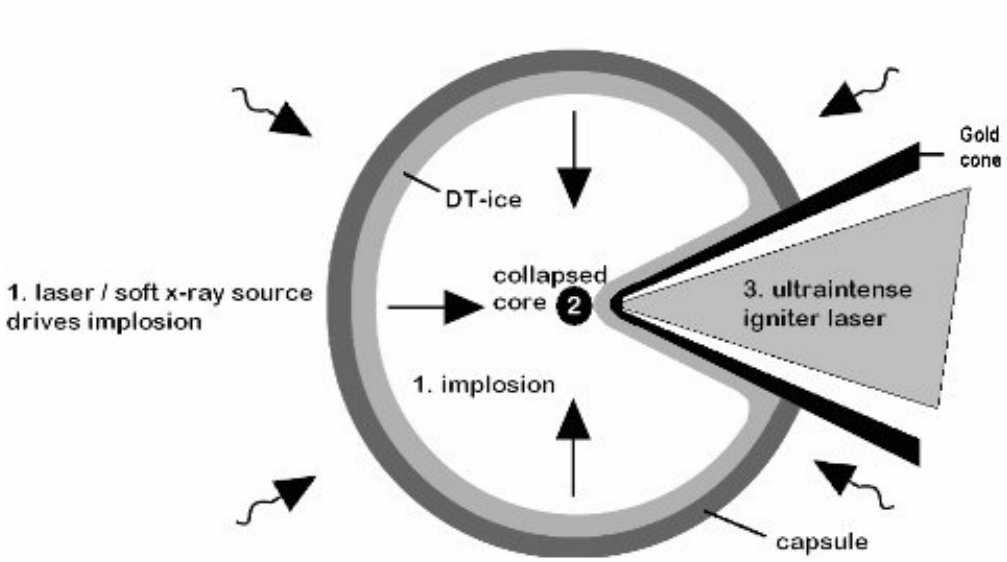

Figure 1.5: Fast ignition scheme [18].

The Fast Ignition is a 3 step process. The implosion is driven by X-rays and as a conseguence a dense fuel spot is generated as shown in Figure 1.5. Then, an ultra-intense laser is focused on an acceleration target leading to the injection of very highly energetic electrons into the fuel, heating the hot spot environment to the conditions close to those required for fusion. In order to inject these electrons an unique pellet design is proposed. A gold cone is inserted into the pellet in order to directly focus the electrons into the hot spot. However, this design leads to a asimmetry of the pellet which deleterial for the compression efficiency. Nevertheless, fast ignition opens a perspective to ignite and burn fuel mixtures which require more severe benchmarks with respect to the DT one.The work by Atzeni and Ciampi [1] has shown that fast ignition of pure deuterium with the help of a DT seed is possible.This can be of great advantage since one of the major technical issues with DT mixture is the neutrons production (contamination, activation, materials embrittlement and so on). Deuterium-Deuterium reaction has two possible channels almost equally likely to occur:

$$D + D \rightarrow T(1,01MeV) + p(3,02MeV) \tag{1.7a}$$

$$D + D \rightarrow 3He(0,82MeV) + n(2,45MeV) \tag{1.7b}$$

As you can see the neutrons produced in this case are much less energetic than those produced by DT fusion, and this is of great advantage expecially for what concerns the embrittlement of structural materials. For what concerns material activation neutrons

are always dangerous because, as Fermi taught us, some nuclear processes which involve neutrons exhibit much higher cross sections for less energetic neutrons. From this point of view one could choose structural materials which poorly react to that specific neutron spectrum.

1.4. The ABC facility

A LASER (Light Amplification by Stimulated Emission of Radiation) is a device able to emits a light beam having peculiar characteristics which are useful for a number of purposes. These characteristics are:

- Monochromaticity: the spectral band of the laser is very narrow, it's color is very pure;
- Coherence: A light source is coherent when the photons it emits ehxibit a constant phase relation. Therefore they interact letting interferences appear. The temporal coherence is related to the amount of time this phase relation remains constant. The spatial coherence is related to the transverse distance along the propagation axis at which the phase relation is still constant;
- Directionality:The solid angle within the light is emitted by the source remains small during the propagation;
- Brightness: It is related to the amount of light emitted by the source within a certain amount of time. It is therefore also connected to the laser intensity.

In order to increase the photon population a laser takes advantage on the stimulated emission phenomena which allows the production of a huge number of photons which have the same wavelength, coherence, directionality and brightness. In order to produce these photons it is necessary for them to easily interact with excited atoms (so once de-exitated emit the clone photon). This equilibrium is also known as population inversion and it can be achieved in the active media. The pumping system is the one devoted for achieving this condition and sustain it for the required time. To select among all the possible directions and frequencies the system needs to be enclosed in a proper optical cavity called oscillator. The cavity is usually composed by two mirrors whose aim is to reflect photons emitted by the active media back to it (so amplifying the photon population). The geometry of the oscillator determines direction and frequency. One of the mirror is not perfectly reflective on purpose: photons allowed to escape from the oscillator are what constitute the laser light. The ABC facility is constituted by two counter propagating lines and each of them can produce a 1054 nm pulse of 100 J energy whose waveform is sin^2, the time duration

is 3 ns at Full Width Half Maximum (FWHM) and a focal spot whose minum diameter is 50 μm due to the diffraction limit. The highest intensity that can be reached is 10^{15} W/cm^2. Such an intensity is comparable to which of a single laser generated by big ICF facilities, such as the National Ignition Facility (NIF) in USA or Laser MegaJoule (LMJ) in France. Along one of the lines we have a beam splitter whose role is to split the beam in order to get another beam in the pre-amplification phase and then sent in a harmonic doubler. At the end of the process this beam exhibits a wavelenght halved, a duration of 0.5 ns and an energy much smaller than the fully amplified beam (in the order of 100 mJ). This green beam is used for diagnostics purposes.

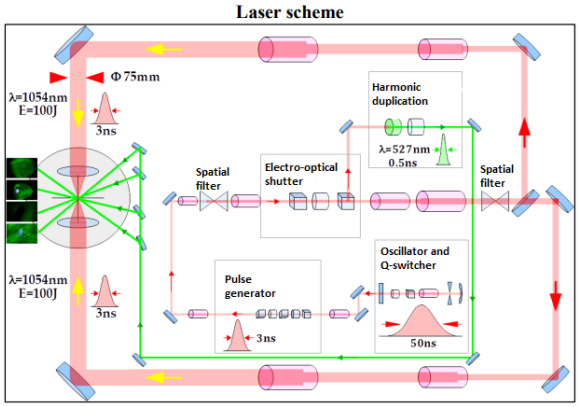

Figure 1.6: ABC scheme (ENEA archive)

Such a laser is always constituted by a number of devices whose final aim is to start with a seed up to an extremely powerful laser beam. To do so many intermediate steps are required, several amplification phases are necessary. Since the pulses produced by this apparaturs are relatively long (in the order of ns) there is no need for pulse compressors. The oscillator generates a seed whose duration is 50 ns. Prior the amplification phases, the pulse generator and the electro-optical shutter are devoted to cut the pulse leaving it to the desired duration (3 ns). The amplification phases are up to neodymium doped phosphate glass bars, which is the active media. In order to allow the active media to act as amplifier we have to supply energy. This is done through flash lamps.

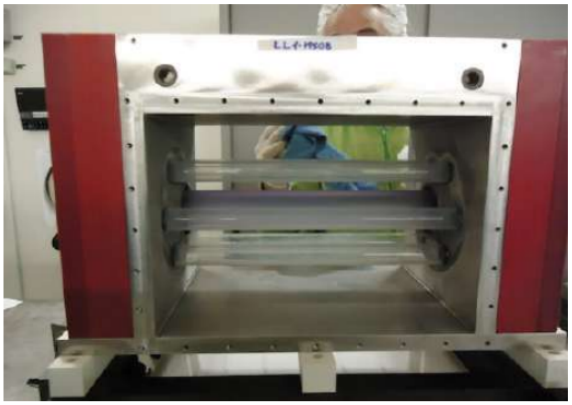

Figure 1.7: This is the amplifier. As you can see the neodymium bar is sorrounded by 4 flash lamps (ENEA archive).

As I am going to show in Chapter 5 and in Appendix B there are several different diagnostics working simultaneosly in each experiments. From this point of view the ABC facility is one of the most equipped worldwide. I will not talk about all the different diagnostics. I will only mention those which are of interest for our purposes. In order to make more clear the discussion I am going to explain some basic concepts about lasers.

Figure 1.8: The laser room. The three tables holding the optical equipment and the amplifiers are visible. The room where the interaction chamber is placed is located on the other side of the wall at the end of the laser room.(ENEA archive).

Figure 1.9: Closed chamber. This is where the target is placed (ENEA archive).

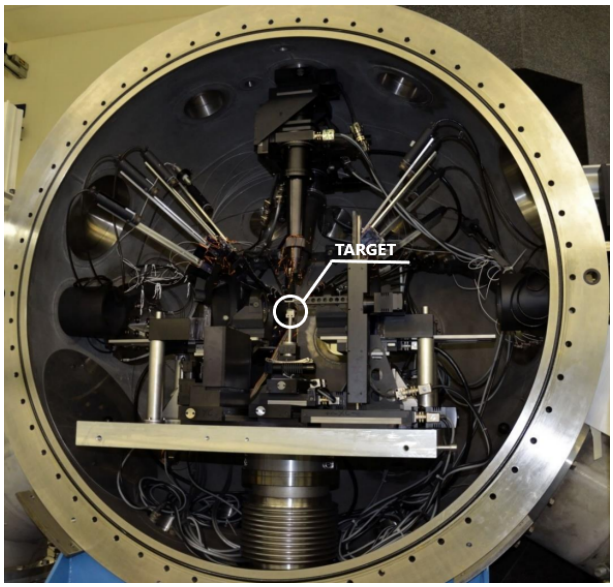

Figure 1.10: Open chamber. The target is visible at the center of the chamber(ENEA archive).

To conclude this section let me summarize the characteristics of the ABC laser in Table 1.1:

Table 1.1: ABC main beam characteristics

Pulse Duration	Intensity	Wavelength	Focal spot size	Energy per pulse
5-6 ns	10^{13-15}W/cm^2	1054 nm	50-100 μm	up to 100 J

2 | Foams materials and their application in ICF

Foams can be seen as porous materials which are promising for use in both the direct (low Z: plastics,carbon) and indirect (High Z: gold, lead) drive inertial confinement fusion targets. In particular, such materials can be used as external components of the target to provide a volumetric absorption of the radiation of laser beams while reducing the irregularities of the absorbed laser energy distribution. The average density of porous materials which are nowadays involved in ICF can vary widely from a few $\frac{mg}{cm^3}$ to several hundreds of $\frac{mg}{cm^3}$. As a matter of fact a foam made of a certain material exhibits an average density which is much lower than the ordinary solid state density of that material. The pore size can vary from a few microns to several tens of microns while the thickness of solid elements varies from a few microns to a few hundredths of microns. The techniques which have been adopted utill now for producing plastic foams lie in the category of chemical deposition. The porous media produced in this way have a mixed filamentous-membrane structure. We usually refer to those foams as *"Micro-Structured foams"*.

One of the goal of this thesis work is to understand the potentiality of producing foams by means of a technique which is very different from the chemical deposition, which is an effective way to produce plastic foams. In particular the Pulsed Laser Deposition (PLD) technique, which is explained in 2.5, may be a reliable and effective method to produce metallic nano-structured foams. To these foams we can refer as *"Cluster Assembled foams"*.

2.1. Materials for ICF applications:Foams

When these materials are irradiated by a high intensity laser, a high-temperature plasma is formed which, for targets made of light elements, is usually fully ionized. Light foams are identified as under/over critical if the average electron density of such media, totally ionized, is smaller/larger than the critical density for the laser wavelength. The properties of absorption and energy transfer in a laser-produced plasma of light element foam strongly depends on the homogenization process of such a medium. The homogenization

time of the plasma created by powerful laser radiation with intensity exceeding $10^{13}\mathrm{W/cm}^2$ is a few tens of picoseconds in the case of small-pore materials and a few nanoseconds in the case of large-pore materials. Until completion of the homogenization process, the absorption of laser radiation occurs in an inhomogeneous plasma with stochastically oscillating density. This effect is particularly important for the absorption of laser radiation in a porous material with density greater than the critical density of the created plasma. This effect, togheter with the geometrical configuration of a foam which exhibits a huge surface to volume ratio, is the cause of 80–90 percent of absorption for a laser pulse of nanosecond duration in a large-pore substance with density larger than the critical one. In the case of small-pore materials with an overcritical density, this effect is important for absorption of laser pulses having a duration of no more than 100 ps. Moreover, all the wave propagation mechanisms are moderated by the precence of the pores [11],[8],[10]. To summarize, foams exhibit peculiar absorption and wave transport properties which are the reason why they are acquiring greater interest for ICF applications. They are, respect to ordinary materials, more efficient in absorbing the laser energy and in converting it into mechanical energy(trasported by shock waves). The most known porous materials of light elements are plastics such as [11]: $([CH]_n, [CH_2]_n)$, agar-agar $(C_{12}H_{18}O_9)$, cellulose triacetate $(TAC, C_{12}H_{16}O_8)$, trimethylolpropane triacrylate $(TMPTA, C_{15}H_{20}O_6)$, and polyvinylalcohol $(PVA, [CH_2CH(OH)]_n)$. Using various chemical deposition methods, porous substances with different structure, average pore size, and density can be obtained (see, for example, Refs. [22] and [17] which are quoted in [11]). These materials are quite well characterized in terms of Equation Of State and Hugoniot adiabat. The Equation Of State is the relation among the thermodynamic variables; temperature, pressure and density. In experiments involving materials ablated by a high-intensity laser the EOS is always evaluated in tabular form. The Hugoniot adiabat is a curve in the p,V plane which links the quantities defined by the jump condition through a shock front A.1(despite the name shock compression is adiabatic only in the limit of weak shocks [36]). In a small-pore(1-10 μm is the usual range to which we refer as small) foams the shock wave, which come from the solid ablator irradiated by a laser pulse, is believed to exibits an Hugoniot adiabat which, in a wide range of density,slightly differs from the adiabat of equivalent ideal gas [16],[12]. This behaviour of the hugoniot adiabat shared by porous materials and ideal gases is an important point which will be exploited in chapter 4. One of the most important aspect which will require additional efforts is to understand to which extend these beheaviours of the *micro-structured foams* can be applied to the afore mentioned *cluster assembled foams*.

So, foams are very interesting materials for the reasons I talked about but potentially

more since their properties are not fully investigated yet.

2.2. Introduction to foams modeling

In this thesis the focus is on porous materials which can be used in ICF applications. In general, these porous materials exibit area fractal internal morphology whose characteristics differ depending on the production method. This fractal structure is related to the presence of pores. Such pores are not necessarily closed empty holes. These pores have to be seen in an equivalent way. TAC foams have been used for long time as a foam in ICF experiments despite the fact that this materials does not exibits real pores but filamentous structures instead.

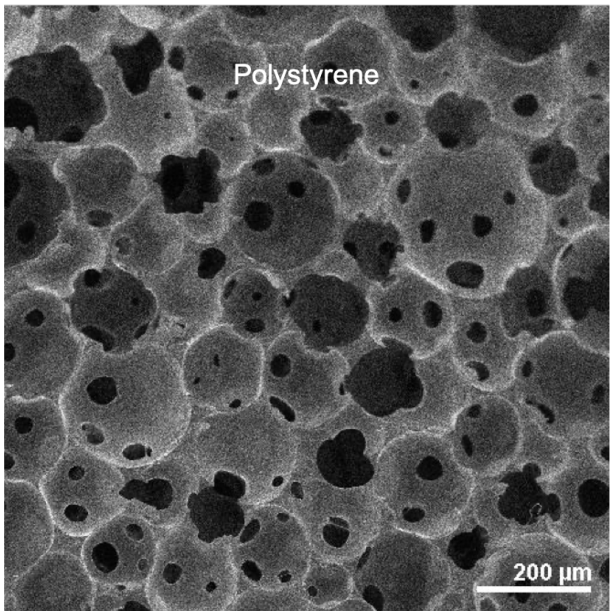

Figure 2.1: This is a typical immagine of a Polystyrene foam. The porous structure is clearly evident (ENEA archive).

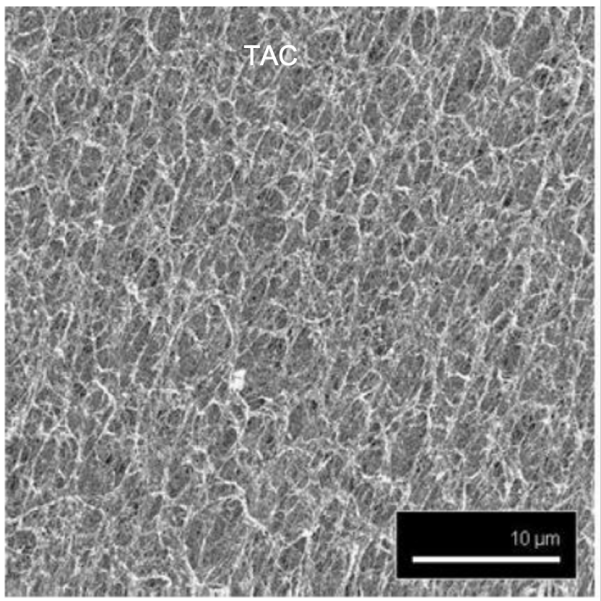

Figure 2.2: This is the TAC. As you can see it exibits a filamentous structure rather than a porous one (ENEA archive).

Despite the differences in their structures both the foams showed above can successfully be descrivber by the Gusk'ov's fractal model [34]. It is a semi-empirical model able to connect pore dimension, solid element thickness, average foam density and solid element density:

$$\begin{cases} \frac{\delta_0}{b_0} = (\frac{\rho_s}{\rho_p})^{\alpha} \end{cases} \tag{2.1a}$$

- $\delta_0 \rightarrow$ pore dimension;
- $b_0 \rightarrow$ solid element thickness;
- $\rho_s \rightarrow$ solid element density;
- $\rho_p \rightarrow$ average foam density;
- $\alpha \rightarrow$ fractal parameter.

$\alpha = 1/(\nu + 1)$ where ν is 0 for planar solid elements, 1 for cylindrical solid elements,2 for spherical solid elements. In the real world there are no pure shapes, they are always hybrids combinations of simpler ones. Porous structures of light elements are promising materials for use in the direct drive inertial confinement fusion targets. The average

density of porous materials can vary widely from a few mg/cm^3 to several hundred of mg/cm^3. When these materials are directly irradiated by high intensity laser, a high-temperature plasma is formed which, for targets of light elements, is usually fully ionized. The pore size can vary from a few microns to several tens of microns while the thickness of solid elements varies from a few microns to a few hundredths of microns. Typically, the porous media have a mixed filamentous-membrane structure, therefore a fractal parameter of about 0.8 (empirically determined). The value of the fractal parameter α is actually an open point since the usual chemical deposition processes do not allow for an a priori control of it. All we can do is to make the foam and then performing experiments having the aim to get α from 2.1. As I will explain later on in this chapter other foam production processes may allow for a better control of α.
Foams are worldwide recognized as materials which show usefull characteristics which allow them to be used in a great number of different applications (Ablators and Hohlraums in ICF, particles generation, particles acceleration and so on). Having said that, the purpose of this thesis is to uderstand if an unsual class of foam can be of our interest. In Politecnico di Milano the NanoLab group produces nanostructured fractal-like materials through the Pulsed Laser Deposition (PLD) technique. We will exstensively talk about them in the next chapter. We will also show a connection (which is one of the results of the collaboration between Politecnico di Milano and ENEA) in between the fractal model written above and the fractal model indipendently developed in [20].

2.3. Carbon foams as ablators

The fuel pellet consists of a hollow shell capsule with an outer ablator layer.To point out which is the order of magnitude of the length in play, the outer radius of the shell is slightly less than 2 mm, and its aspect ratio (radius to thickness ratio) is about 10. The central cavity is filled with the fuel mixture vapour, which forms part of the ignition hot spot after the implosion [36]. As shown by experiments performed at the NIF facility carbon ablators are attractive[3, 4, 14]. The published results are mostly about High Density Carbon(HDC), which is the most promising ablator material under investigation rigth now. The open problems related to the ablation phase of the fuel pellet are related to: compression symmetry, efficiency of absorption, final pressure. Despite HDC exibits good performances a lot of technical issues,related to the aforementioned open problems, are still very difficult to be outdated. Therefore an analysis about carbon foams can be for sure of interest due to all the peculiarities concerning foams. What is known about foams is almost entirely related to the interaction between high intensity lasers and plastic foams produced through chemical deposition processes [17, 22]. A plastic foam exibit

respect to a bulk plastic target a higher absorption efficiency, better implosion symmetry and a much higher final pressure [8, 11]. Since plastics generally exibit electromagnetic properties which are not so distant from those of carbon we may expect that similar improvements can be achieved by considering carbon foam instead of a HDC. A whatever plastic is a combination of hydrogen atoms, carbon atoms and sometimes oxygen atoms (where carbon always constitute a big portion of the aggregate). Moreover the overall atomic number Z is small and this means that in both a plastic foam and a carbon foam the radiation field coupling with the matter can be neglected. Foams represent a new frontier of ablator materials which is not fully understood yet. Pure carbon foams are a completely novel class of materials since there are no systematic analysis of their properties once irradiated by an high intensity laser. All can be said at this moment of the discussion is that, since the already known properties of plastic foams we expect a similar behaviour of the carbon foams for two reasons. First, different plastics are generally made of hydrogen and carbon atoms in different proportions therefore something about the carbon effect can for sure be inferred. Second, the physics involved for the ablation development is the very same; hydrodynamics and heat transport is all we need to talk about the physical characteristics of the phenomena. Indeed, since plastic and carbon are both low Z materials we can completely neglect the effect of the coupling between the radiation field and the matter. These are the reasons behind the assumption that a carbon foam may behaves similarly to a plastic one while exibiting better characteristics for the ablation purposes. The foam version of carbon is expected to be more efficient in converting the laser energy into mechanical energy available for a strong shock formation respect to an HDC ablator. The role of the pores is a central one. Having an internal porous structure leads to an improvement in terms of pressure levels. This fact can be explained by considering that the shock propagates slower in a foam (respect to an ideal homogeneous material having the same density) due to the precence of the pores. Moreover the shock formation itself is delayed due to the internal structure; the energy absorption develops in a smaller volume. This effect depends on the pores dimension; The bigger the pores the slower the shock formation so the higher the pressure. Also the symmetry of the implosion is expected to be better than an ordinary material [11].

2.4. Gold foams as X-ray radiator: Hohlraum

For what concern gold is already well known that high-Z materials are not good ablators. Since the radiation field in the gold case is not negligible unavoidably a big amount of energy is absorbed by the photon field. This will act as shock suppression. Hovewer gold exhibits an high capability of converting the laser energy into X-rays. This is the

reason for adopting gold for making an hohlraum, since in the indirect scheme we look for a compression which must be as much as possible isotropic. Among all the high-Z materials which could be used gold is the one which simultaneosly satisfies the most important physical and engineering requirements, in order; conversion efficiency, easy crafting. In [25] is shown how a lead hohlraum exibits an indistinguishable conversion efficiency respect to that of gold being much less expensive. The use of lead would reduce the overall cost of the targets of at least 30 percent. Nevertheless gold is a much more investigated material, whose behaviour under irradiation is well known and so most of the scientific community agrees on its use for this kind of applications. In support of this fact I can also say that in the tabular equations of state database to which I had access there are 5 EOS for gold (each of them obtained for specific irradiation conditions) but none for lead. So, due to this features which has been verified by my simulations too (as I am going to show in chapter 4), an high-Z material is not the ideal for making an ablator, whose role is to convert as much as possible laser energy into mechanical energy. Nevertheless recent works by [32] has demonstrated the feasability of using low density foam gold as radiator for making an efficient hohlraum.By a proper choice of the laser parameters an higher conversion efficency into X-rays can be achieved. The hohlraum is used since it is able to ensure a sufficiently symmetric capsule drive. In fact black body radiation is uniform and isotropic by definition and therefore ideal to drive a spherical implosion. The detailed energy distributions and plasma profiles for laser-irradiated solid gold and gold foam targets were studied by using MULTI-FM 1D (which is the same tool I am going to explain in chapter 3 since I used it for carrying out the simulations proposed in my thesis work). This study ([32]) shwon that the radiation heat wave is subsonic for the solid gold target, while supersonic for the foam gold target. In the latter case, the shock wave is behind the supersonic radiation heat wave. This generates a gradient in the plasma temperature profile with higher temperatures near the shock wave which result in an enhancement of the x-ray emission.

However these simulations [32] do not consider any internal structure for the gold foam. Of course these notions are well understood by the ICF community. What I am proposing in this thesis is the analysis of foam gold,so an analysis which takes into account the internal strcture of the foam. Only few articles are devoted to this subject: [13],[32], but still none of them takes into account for the internal structure of the foam. Last but not least, these gold foams which are under investigation by the group of the latter quoted work can be produced by the NanoLab group through the Pulsed Laser Deposition technique.

2.5. A way to produce novel foams:Pulsed Laser Deposition (PLD)

As I already said at the beginning of this chapter, ordinary micro-structured low-Z foams are produced through chemical deposition techniques. These do not allow for an active control on the fractal parameter α. The capability of having a real control on this key parameter is just one of the potential advantages of using Pulsed Laser Deposition, since we are going to show that due to the fractal models analogy a connection can be enstrablished leading to an higher control degree on the foam characteristics. Moreover the PLD techniques is adequate for producing high-Z foams, while the chemical deposition is not. Lastly the PLD allows for a higher purity level of the produced foam (oxygen and hydrogen contamination are unavoidable in any case once the target is exposed to the atmosphere, also considering the high surface to volume ratio). Let us recall that foams produced through PLD are often referred as nano-foams, but from we can more precisely refer to them as Cluster-Assembled foams. These foams lie in a class of materials characterized by a large fraction of sub-micrometric voids and/or pores (typically $>= 90\%$). Nanofoams exhibits densities in the range $1 - 100 mg/cm^3$, an extremely high surface-to-volume ratio. These characteristics make make them of interest for many research fields: hydrogen storage, supercapacitors and catalysts, water treatment, gas sensing, and medicine [20], [21]. For this work we want to make clear that we are trying to figure out if among all these applications we can add another one; ablators and hohlraums for ICF. PLD is a well enstablished material production technique. It can be used in a broad range applications, allowing the production of a number of different kind of substrates. PLD can be exploited to produce carbon cluster assembled foams, with controlled and reproducible mean density and high purity level. It's well understood that PLD carbon cluster assembled foams exhibit a fractal like structures made of carbon nanoparticles, whose average radius range in the order of 1-10 nm. There two approaches to the PLD whose difference is the ablation regimes: nano-second and femto-second ablation. Production of nanoparticles has been observed both in nano-second and femto-second regimes but there are a lot of differences which make them suitable for specific purposes.

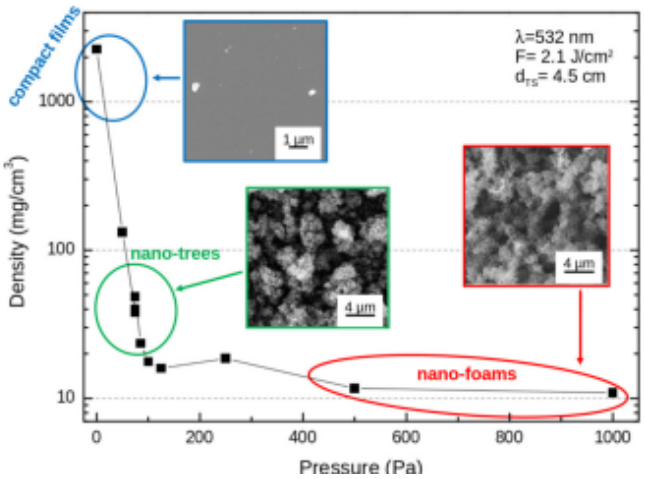

Figure 2.3: This figure shows the average density of a PLD carbon films by varying the BKG argon pressure [19].

There are a lot of specialized articles for what concern the synthesis of a nano-particle. The efforts made by the Polimi Group was to understand the physical mechanisms acting in the aggregation of such nanoparticles. The working principle is the very same in the two deposition regimes. The deposition process is achieved in a chamber whose environment is well characterized. A target of the material of interest and the deposition substrate (whose composition is not whatever, in fact in [20] has been shown that the aggregation process of the nano-particles into clusters mainly occurs in flight) are placed into the chamber at a given distance and a given BKG pressure (usually an argon environment). A laser ablates the target from a well defined direction. A plume of material is developed. The laser fluence (so repetition rate,energy per pulse, pulse duration, spot area) is the other parameter which together with the target to substrate distance and the BKG composition (pressure and chemical composition of the gas) plays a role into the foam generation. According to [20], an experimental and modelling investigation of the physics underlying the growth of carbon cluster assembled foams in nanosecond PLD has been proposed. As I already mentioned the physics of how nano-particles are synthetized is well known. We are going to explain the nano-particles aggregation mechanisms which lead to a certain deposited structure. Basically in nano-second laser ablation (which is usually characterized by a repetition rate which is another important parameter influencing the deposition) we can consider two main possibilities: aggregation on substrate and aggregation in flight (so into the plume). Typical PLD experiments can be classified into two regimes distinguished according to the duration of laser pulses, which in turn determines the physics of laser ablation dynamics which depends on the ablation regime; in the ns regime the thermal ablation which takes place is a well understood process while

in the fs regime we have to deal with an electronic ablation dynamics which is still matter of research. Moreover, the height of some aggregates is in the order of their lateral size, therefore much larger than the nano-particle size. A 2D aggregation process, such as Diffusion Limited Aggregation Substrate DLAS), is unlikely. In [21] a *snowfall* model to describe the nanofoam growth (by using a pyrolitic carbon target) in the ns-regime has been proposed: molecules, atoms and nanoparticles(in a small but non zero fraction) are promptly ejected from the target. These species expand into BKG gas and due to the cooling down nanoparticles are generated. Once the nanoparticle's population reach a certain saturation level they begin to stick each other leading to the formation of micrometric fractal-like aggregates. This process is known as Cluster-Cluster Aggregation Mechanism (CCA). Once these fractal-like aggregates land onto a substrate the foam starts to be generated.

2.5.1. Comparison between different PLD deposition regimes

In [21] a comparison between ns and fs regimes is shown through SEM micrographs as a function of the argon background pressure and the laser fluence respectively. As a matter of fact since the two regimes are characterized by different time pulses in order to have the same laser fluence the spot size is properly tuned. In high vacuum condition, at least below 10^{-3} Pa (which is not shown in the figures below), no aggregates nor nanoparticles could be seen on the substrate. A compact, near bulk density, flat, homogeneous films is obtained for both deposition regimes: the ablated species can travel freely in high vacuum, reaching the substrate with considerable energy. The slowing effect of a background gas together with the stronger plume confinement are responsible for the clustering of single nanoparticles into fractal-like aggregates.The background pressure therefore plays a central role in controlling the characteristics of the fractal aggregate. As shown in [21] in both deposition regimes the peculiar nanofoam structure is determined by the properties of fractal-like aggregates of nanoparticles. The nanoparticle dimension, in the order of 10 μm (8 μm for the fs-PLD and 10 μm for the ns-PLD), resulted to be relatively independent from fluence and pressure. Moreover, the analysis of the distribution of fractal-like aggregates showed that two different aggregate populations can be distinguished in the case of fs-PLD, which something which does not happen in the ns-PLD. The study of fractal dimension indicates that the growth mechanism of carbon nanofoams is essentially the same in both deposition regimes,so an in-flight cluster-cluster aggregation process, which is in between the diffusion-limited and reaction-limited aggregation processes. In conclusion, is it possibile to finely tune and control the carbon nanofoam properties by acting on the deposition parameters in both PLD regimes. The fs-PLD technique can represent

a reliable alternative to the standard fs-PLD for the production of carbon nanostructured materials. An important difference arise by taking into account the crystalline structure(), nanoparticle dimensions and spatial uniformity(we know that in the fs-PLD two populations of aggregates which exibit different characteristics are formed). As a matter of fact the two techniques can be considered complementary.

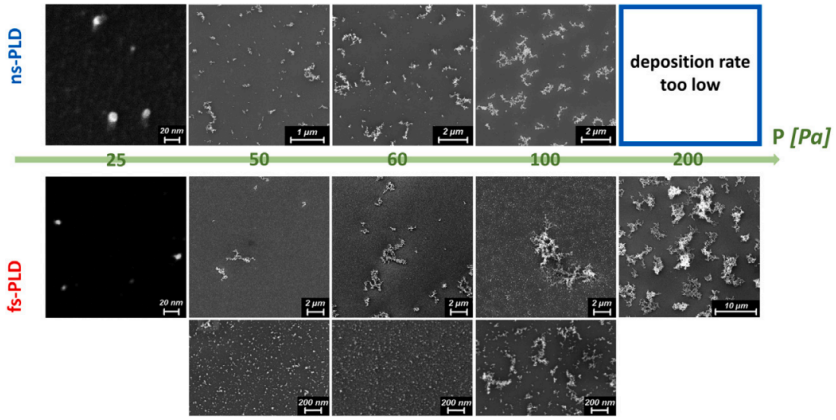

Figure 2.4: Scanning Electron Microscope (SEM) images of a carbon fractal aggregates, obtained with short deposition times (30 s) and displayed as a function of the background argon pressure at a given fluence [21].

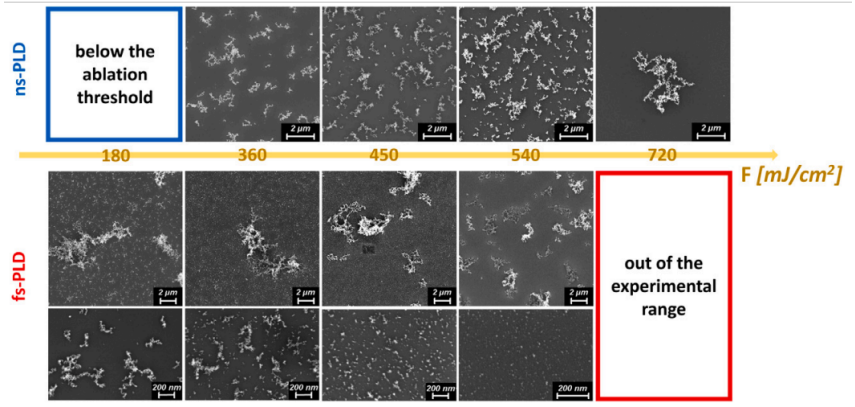

Figure 2.5: SEM images of a carbon fractal aggregates, obtained with short deposition times (30 s) and displayed as a function of the fluence at a given background argon pressure [21].

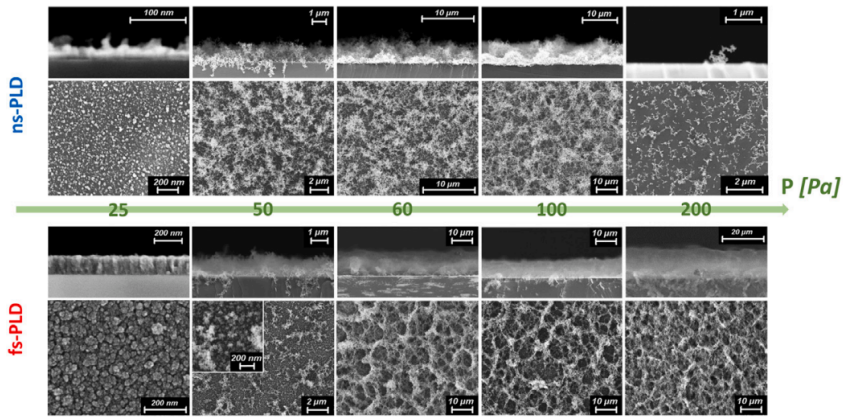

Figure 2.6: SEM images of a carbon fractal aggregates, obtained with high deposition times (10 min) and displayed as a function of the background argon pressure at a given fluence [21].

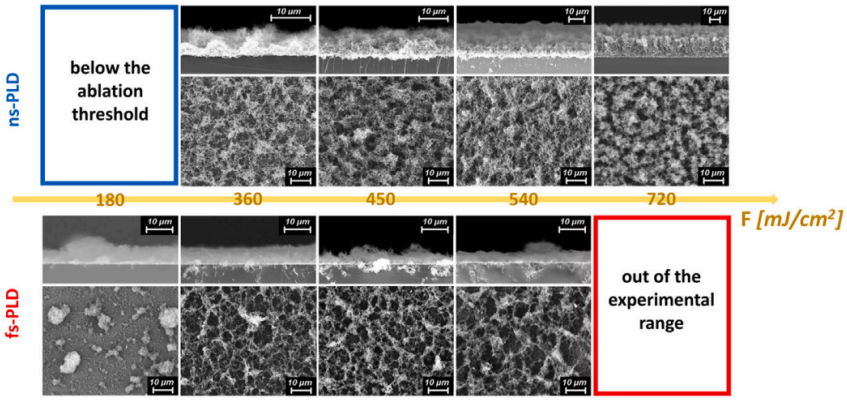

Figure 2.7: SEM images of a carbon fractal aggregates, obtained with high deposition times (10 min) and displayed as a function of the fluence at a given background argon pressure [21].

Let us compare figures 2.6 with 2.1 and 2.2. As you can see by increasing the pressure the internal structures of the ns-PLD and fs-PLD foams are close, respectively, to that of TAC and Polysterene. Moreover by comparing 2.7 with the internal structures of polysterene and tac the situation is quite similar. The structure of the fs-PLD foam looks like very similar to the previous one. The structure of the ns-PLD foam is significantly affected by this change but it is still closer to the tac's strcture. Other technical details concerning the difference of these techniques in relation to the use in the ICF context will be discussed in Sections 5.1,5.2 where the analysis of the design of carbon and gold target will be carried out.

2.5.2. Fractal's models analogy

Carrying out the thesis work some analogies between the so called Gusk'ov fractal model(equation 2.1) and what is actually done through the PLD technique. In fact let us recall the already mentioned Gus'kov model:

$$\rho_s = \rho_p \left(\frac{\delta_0}{b_0}\right)^{\nu+1} \tag{2.2}$$

Let us compare this formula to the fractal model which is shown in [21]:

$$N = K \left(\frac{R_g}{R_{np}}\right)^{D_f} \tag{2.3}$$

Where:

- N is the number of nanoparticles composing the aggregate;
- K is an empirical factor in the order of unity;
- R_g is the giration radius defined as the radius at which a number of filled spaces equal to that of the entire pattern would have to be placed to have the same moment of inertia [21];
- R_{np} is the nanoparticle's radius;
- D_f is the fractal dimension,which is a measure of the space filling capacity of a pattern/system, and tells how a fractal scales differently from the space it is embedded in [21].

These two model has been develped by the authors indipendently. A connection between them can be put in evidence though the following reasoning.

- V=(Nanoparticle volume)N=volume of the aggregate;
- m_{np}=Nanopartcile mass;
- f=filling factor;

Let use further assume:

$$\frac{N m_{np}}{V} = \frac{m_{np}}{V_{np}} = \rho_s \tag{2.4}$$

$$\frac{N m_{np}}{V} f = \rho_p \tag{2.5}$$

Let us remember that ν assumes the values 0,1 or 2 depending on the solid element structure. Due to the fractality of the aggregate it can assume non integer values from

0 to 2. On th other hand D_f is a quantity whose values is 1,2,3 depending on the dimensionality of the aggregate. Due to the fractality of the aggregate it can assume non integer values from 1 to 3. My guess is to set $D_f = \nu + 1$. If legit it would imply a direct link between the pore dimension and the giration radius, which are the main reference quantities of the two models.

$$\delta_0 = R_g \left(\frac{b_0}{R_{np}}\right) \left(\frac{K}{fN}\right)^{1/D_f} \tag{2.6}$$

One should perform two indipendent experiments with the aim of verifying if the two sides of the equation written above do coincide. A first approach can be the following one. Under the hypohtesis that the exhibits a clear porous structure we can easily measure the pore dimension through a proper microscope (SEM imaging is adequate). This would be the case of a foam made of polysterene, whose internal structure has been shown in 2.1. This give us a measure for the left hand side of 2.6. The same approach can be adopted to have a measure for the solid elements thickness b_0. The remaining part of the right hand side 2.6 must be determined by the specific characteristics of the deposition:

- R_g is the gyration radius which can be measured as the radius of the circle with area equal to the aggregate effective area, which is obtained from the binarized aggregate immage [21];
- R_{np} is the nanoparticles radius depends on the deposition regime;
- K is a semiempirical tuning factor which depends on the speficid charateristics of the deposition;
- f is the filling factor, which can be measured as the ratio $\frac{\rho_p}{\rho_s}$;
- N is the number of nanoparticles constituting the whole aggregates which is a parameter which depends on the deposition regime and laser/BKG characteristics ;
- D_f is the fractal dimension which can be measured through a numerical approach starting from a 2D SEM immages of the aggregates [21];

So, we have all the elements for performing the measurements of the quantities appearing in 2.6. If the foam of interest exhibit a TAC-like internal structure 2.2 (so if we use the PLD it would quite likely the result of a ns-PLD deposition) the situtation gets worse. In this case we would not have any direct method for measuring the pore's dimension since these pores do not exist in reality but only as a math-tool. The only way in this case is to go for a trial and error procedure. We have first to get an existimation of this equivalent pore dimension and this can be done by ablating many targets having the same charac-

teristics and comparing the experimental results with numerical results. The simulations have to be performed each time assuming all the same parameters except for the pore dimension which is the free variable we are trying to determine. Once experimental data and simulations converge, within an accepted error,we get the pore dimension. Moreover in this situation we may also have an indipent extimation/measurement of the fractal parameter α. So we need to use a foam whose α is known and then measures the quantities listed above. Such a comparison has never been conducted and it represent one of the original theorerics contributions of my work.

2.6. Aims of the work

Nowadays carbon and gold are studied due to their promising properties in ICF applications, in particular, to be used as ablators and hohlraum constituents, respectively. In my thesis, both these applications will be considered and I will separately discuss carbon foam ablators and gold foams as X-ray radiators for hohlraums. The motivations of the work are a consequence of the current state of these technologies, which has been pointed out in sections 2.3 and 2.4, in relation to the PLD technique (Section 2.5) which can be used for the production of novel foams. The overall purpose of this thesis is to investigate new directions in the use of foams since to our knowledge there are no previous studies on carbon foam ablators nor on gold foam hohlraums, which take into account the porous internal structure, available in literature. This is the starting point of my original contribution. The study of the properties of the physics of the interaction between a high intensity laser and a foam is the core of my work. An important aspect consists in the understanding of how PLD can be used for making both carbon ablators and gold hohlraums, since this technique has been not completely exploited to its full potential for ICF applications. As explained in 2.5 there are different deposition regimes and depending on the desired properties of the target (which comes from the simulative work carried out in order to optimize them) one may use a ns-PLD or a fs-PLD. This analysis will be shown in the respective paragraphs dedicated to the targets design in chapter 5. For what concerns the part of the work related to the analysis of the materials let me consider carbon foams first. All the articles available at the moment concerning the use of foams as ablators consider plastic foams. There are no studies about a carbon foam ablator, independently on manufacturing technique adopted. The first part of the fourth chapter has the aim of extending our understanding of the physics related to the interaction of a carbon foam and a high intensity laser. This will be achieved through simulations performed with the MULTI-FM radiation-hydrodynamic code (Chapter 3), especially developed for modelling this kind of interaction. This analysis will identify the

possible advantages of using a carbon foam ablator instead of a HDC ablator. It is worth to be noted that, despite the fact that HDC is already used in these applications, there are no available simulations performed with MULTI-FM which show its properties under irradiation, and so what will be shown about carbon foams in chapter 4 will be a fully original work. In chapter 5 I will show an optimized ablator design of a carbon foam target, taking into account the typical irradiation conditions of the ABC facility (see Section 1.4) and optimized parameters for maximizing the final pressure, which is the most important quantity which must be improved. This design has the aim of showing to which extend a carbon foam can perform better than a HDC one. To conclude this part of the analysis I will present the design of an experiment to be realized at the ABC facility whose aim is to compare the compression performance of different ablators, which is related to the pressure. The adopted technique consists in measuring the dimension of the crater generated onto an Aluminium slab placed on the rear side of the foam target. This will give us an evaluation of the capability of the foam of converting the laser energy into mechanical energy. This technique, which is well validated for plastic foams ablated by a high-intensity laser (as explained in [11]), has never been used in experiments involving carbon foams. For what concerns the study of gold foams for their potential use as hohlraums, as shown by the numerical work reported in [32], Low Density Gold (LDG) targets exhibit higher conversion efficiencies of the laser energy into X-rays respect to a gold target of ordinary density. However, there are no theoretic nor experimental works which properly take into account for the internal structure of the material. This is a crucial limitation and it is also the starting point for the work I will develop in chapter 4 concerning gold foams. The code I will adopt (again MULTI-FM) is the very same used in [32] and so I will have the opportunity of realizing a full comparison between their results and mine, in order to verify the goodness of my results. Then I will perform simulations properly considering the internal structure of the target, which will allow us to understand why and to which extend a gold foam exhibits better conversion performances respect to an ordinary gold target. In chapter 5 I will design an optimized gold foam target having the aim to ablate it at the ABC facility and then I will also show how to experimentally verify if these foams are actually more efficient. To conclude, in chapter 6 I will extensively talk about the future developments in relation on the state of the art and the results of my work. The aim will be to explain how my results can be improved through future upgrades of the code and of the physical models. Let me summarize the aims of the work:

- The investigation of the potentialities of the PLD technique for making foams for ICF applications, such as ablators and hohlraums;
- The comparison between HDC and a carbon foam target of the compression perfor-

mance and so the physical mechanisms which takes place into the irradiated carbon foam;

- The comparison between HDG and a gold foam target of the energy conversion performance and so the physical mechanisms which takes place into the irradiated gold foam;
- The design of an optimized carbon foam target for achieving higher compression performances;
- The design of an optimized gold foam target for achieving higher energy conversion performances;
- Investigate the new possibilities given by the use of innovative materials for ICF.

3 | A numerical hydrodynamical tool for laser foam interaction: MULTI-FM 1D

MULTI-FM is a 1D radiation hydrodynamics code [28, 29]. It can be used to simulate the laser-matter interaction in the typical regime of interest for ICF. The very first version was a single fluid model and the absorption was entirely due to the inverse bremsstrahlung. Through the years the code has been upgrated in a two-fluid model. Recently the MULTI-FM code has been developed for reproducing the laser absorption and plasma behavior with porous media also specialized by using an effective absorption coefficient [8] in order to take into account for foams. The code demonstrated a good agreement with the experimental data [9].

3.1. Code description

The equations of radiation transfer coupled with Lagrangian hydrodynamics are solved using a fully implicit numerical scheme. Frequency and angle dependence is included via multi-group treatment. A time splitting algorithm is adopted which feeds in all the groups consecutively during one hydrodynamic time step. The physical phenomena are treated successively during the time step. The numerical stability is guaranteed by using a fully implicit method in every substep. Athough a time-splitting scheme has only a first order accuracy, several advantages justify its use, namely:

- Since the hydrodynamic equations are solved implicitly,the Courant limit in the time step usually found in the explicit schemes can be exceeded (not ignored);
- The necessary numerical work increases only linearly with the number of photon-groups (in simultaneous resolution schemes this increase occurs quadratically);
- A modular design is implemented.

For many problems it is more convenient to choose spatial coordinates comoving with the

material and specifying individual fluids elements rather than fixed points in space. This leads to the Lagrangian representation. It's of particular advantage in situations when the material strongly compresses and when one has different species and needs to follow interfaces. In order to use this approach, one recasts the equations using the positional lagrangian mass coordinates, often written as m, and defined by $dm = \rho(x,t)dx$. On the other hand simple Eulerian codes can handle arbitrary motions of the material but, they are intrinsecally diffusive. Once the material enters a cell it is distributed evenly across the cell. Then, in the next time, step some of this matter can move by another cell. This introduce a non physical enhancement of the mass diffusion. One way to minimize these effects is to locate many cells at regions where materials meet or where gradients are steep. This can be done by using a moving grid.Moreover, since the mesh does not move in an Eulerian scheme, the particles ablated from the target surface are lost as a result of plasma expansion, which can reach distances much larger than the target thickness. Instead, in simple Lagrangian codes the mesh follows the motion of the material, allowing a better description of systems involving a number of components with different properties, which is a common situation in high-energy-density experiments.However Lagrangian codes do not allow diffusion, which is not always an ideal situation. Nevertheless, they are important tools for one dimensional modeling of experiments, even though in two or three dimensions they cannot follow vortical motions.In fact, the formation of a vortex implies the movement of matter from one zone to the other. This could result in overlapping zones, with a node belonging to a cell overtaking another node, so that the new cell is no longer rectangular but is instead tangled. For what concerns the structure of the program, it is written in a modular way with interchangeable modules. The program uses the cgs unit system, with the exception of the unit for the temperature which is eV.

3.2. Model and approximations

The MULTI-code assumes one-dimensional plane symmetry. The gas dynamics equations for velocity v, density ρ, electron specific energy e_e, and ion specific energy e_i, are [29]:

$$\frac{\partial \rho}{\partial t} = -\rho^2 \frac{\partial v}{\partial m} \tag{3.1a}$$

$$\frac{\partial v}{\partial t} = -\frac{\partial (P_i + P_e + P_\nu)}{\partial m} \tag{3.1b}$$

$$\frac{\partial e_e}{\partial t} = -P_e \frac{\partial v}{\partial t} - \frac{\partial q}{\partial m} + \frac{E_{ei}}{\rho} + \frac{S_e}{\rho} + \frac{Q}{\rho} \tag{3.1c}$$

$$\frac{\partial e_i}{\partial t} = -(P_i + P_\nu)\frac{\partial v}{\partial t} - \frac{E_{ei}}{\rho} \tag{3.1d}$$

Where P^e, P^i are the electron and ion pressures respectively, P^ν is the viscous pressure, artificially introduced in order to numerically smooth shock fronts, q is the thermal flux, $E_{ei} = \frac{3\nu_e m_e n_e k}{m_i}(T_i - T_e)$ is the power per unit volume transferred from electrons to ions,where k is the Boltzmann's constant, ν_e is the electron collision frequency, n_e is the electron number density,m_e and m_i are respectively electron mass and ion mass, T_e and T_i are respectively electron and ion temperature. S_e is the deposition of the laser and Q is the total emission rate per unit volume.
These equations 3.1 are valid under the following assumptions:

- Both electrons and ions have the same macroscopic fluid velocity v. This implies that electric currents and magnetic fields are neglected. This approximation is justified in usual situations occurring in laser plasma experiments;
- The radiation pressure contribution into the momentum balance is neglected;
- The viscous effects are entirely due to the ions since the work done by the electron viscous stress tensor is negligible;
- The heat conduction is entirely due to the electrons according to the Spitzer's model. The collisional mean free path of the electrons must be much smaller than the ratio $\frac{T_e}{|\vec{\nabla}(T_e)|}$ (this is not true and in fact the code uses numerical interpolations).

In order to close the system an equation for the radiation field to be coupled to the matter and an Equation Of State (EOS) are needed. Let us consider the radiation field first. We can imagine to state the photon conservation through the radiation transport equation. In the most general case we can write:

$$\left(\frac{1}{c}\partial_t + \vec{n}\cdot\vec{\nabla}\right) I(\vec{r},\vec{n},\nu,t) = \eta(\vec{r},\vec{n},\nu,t) - \chi(\vec{r},\vec{n},\nu,t) I(\vec{r},\vec{n},\nu,t) \tag{3.2}$$

Where I is the specific intensity of radiation of frequency ν at a position $\vec{r}$ traveling in the direction $\vec{n}$ at time t, η is the total emissivity and χ is the total opacity. The term on the right hand side is the effective rate of energy emission (emission minus absorption) by the matter per unit of volume, frequency and solid angle. The total emission rate per

unit volume of energy Q is obtained by integrating over all the frequencies and directions:

$$Q = \int_0^{+\infty} \int_{4\pi} (\eta - \chi I) d\vec{n} d\nu \tag{3.3}$$

I want to highlight the fact that the quantity Q, togheter with the BC (as I am going to show), realize the bridge between the matter and the radiation field. Under the assumption that scattering is not important(precisare come e perché) the emissivity may be written as:

$$\eta(\vec{r}, \vec{n}, \nu, t) = \chi(\vec{r}, \vec{n}, \nu, t) I_S(\vec{r}, \vec{n}, \nu, t) \tag{3.4}$$

Where I_S is the source function. Under conditions of local thermodynamic equilibrium (LTE) Kirchhoff's law is valid and I_S becomes equal to Planck's function (T is the matter temperature)

$$I_p(T, \nu) = \frac{2h\nu^3}{c^2} \left(\exp \frac{h\nu}{kT} - 1 \right)^{-1} \tag{3.5}$$

Deviations of I_S from I_P may become important in laser plasma problems, in particular in the plasma corona, which is a region close to the ablated surface. Most of the available literature devoted to radiation hydrodynamics assume valid the LTE hypothesis. The problem is actually a very complex one. In the paper [7] this problem has been formalized. The most popular criterion used in the literature is the so-called McWhirter criterion, which defines the minimum electron number density which needs to be present in the plasma in order to warrant the existence of LTE.

Moreover, The velocity of the matter is assumed to be small in comparison with the light velocity. Consequently the opacity and the source function can be considered as isotropic (neglecting Doppler effect). In addition they are assumed to depend only on the frequency and the thermodynamic properties of the matter: temperature T and density ρ. This is obviously correct for thermodynamic equilibrium and is the simpler choice for more complicated situations.

Since here we are neglecting all the relativistic effects we can assume the radiation transport as istantaneous once coupled to the fluid equations. Moreover, MULTI-FM is a 1D code. Therefore we can write the radiation transport as:

$$\mu \partial_x I(x, \mu, \nu, t) = \chi(T, \rho, \nu)(I_S(t, \rho, \nu) - I(x, \mu, \nu, t)) \tag{3.6}$$

Where μ is the cosine of the angle between the photon direction and the x axis. In

lagrangian coordinates it reads:

$$\mu\partial_m I(m,\mu,\nu,t) = \frac{\chi}{\rho}(T,\rho,\nu)(I_S(t,\rho,\nu) - I(m,\mu,\nu,t)) \tag{3.7}$$

Where $\frac{\chi}{\rho} = \theta$ is the opacity expressed in units of surface per mass. The above equation is very complicated; the specific intensity depends on four variables. Careless discretization can easily lead to an enormous amount of computational work or a substantial loss of accuracy. The approach adopted here carries out the discretization in two steps. First of all eq. 3.7 is replaced by its integrals over the variables ν and μ in a finite number of domains called 'groups'. This procedure leads to a finite number of differential equations involving a finite number of variables depending only on m and t. In the second step, this set of equations together with the fluid, thermal flux and laser equations is discretized in a computational mesh in the (m,t) space, generating finite difference equations. Let us consider the set of possible pairs of values (ν,μ) of frequency $(0 < \nu < +\infty)$ and cosine $(0 < \mu < 1)$. This set can be partitioned in a finite number NG of subsets that will be called here 'groups' (although properly speaking a group is formed by the photons whose frequency and cosine belong to such a subset). The groups considered here are defined by two boundary frequencies $\nu_a^k < \nu_b^k$ and two boundary cosines $0 < \mu_a^k < \mu_b^k$, where the superindex k stands for the number of the group. The group k is thus the set of photons whose frequency verifies $\nu_a^k < \nu < \nu_b^k$ and whose cosine verifies $\mu_a^k < \mu < \mu_b^k$ (photons travelling to the right) or $-\mu_b^k < \mu < -\mu_a^k$ (photons travelling to the left). It is assumed, of course, that the groups do not overlap and that they cover the whole ν,μ space. It proves convenient to introduce first a few definitions. If f is an arbitrary function of the variables m,ν,μ and t, it can be transformed into a function of (m,t) only through the use of the integral operators $L_+^k, L_-^k and L^k$ defined by:

$$L_+^k(f) = 2\pi \int_{\mu_a^k}^{\mu_b^k} \int_{\nu_a^k}^{\nu_b^k} f(m,\nu,\mu,t) d\nu d\mu \tag{3.8a}$$

$$L_-^k(f) = 2\pi \int_{-\mu_b^k}^{-\mu_a^k} \int_{\nu_a^k}^{\nu_b^k} f(m,\nu,\mu,t) d\nu d\mu \tag{3.8b}$$

$$L^k = L_+^k + L_-^k \tag{3.8c}$$

The last of these operators is the integration over all the frequencies and angles in the group k. The density of the energy U_k and the energy flux S_k of photons belonging to the group k can be expressed as:

$$U_k = \frac{1}{c} L^k(I) \tag{3.9a}$$

$$S_k = L^k(\mu I) \tag{3.9b}$$

Analogously the rate of energy emission per volume by the photons of this group is given by:

$$Q_k = L^k(\chi(I_S - I)) \tag{3.10}$$

and conseguently the total rate is computed adding all the groups. In order to obtain the $group - k$ equations, the radiation trasport equation is integrated separately over the photons travelling to the right and over the photons travelling to the left. This is done by applying the operators L^k_+ and L^k_- respectively. In order to make these equations useful it's necessary to make some reasonable assumptions about the form of the function I. Between the wide range of possible choices, I is selected such that one is able, with a reduced number of groups, to manage situations near the thermodynamical equilibrium with a reasonable accuracy.

$$I = I_P - \mu \frac{1}{\theta} \frac{\partial I_p}{\partial T} \partial_m T + ... \tag{3.11}$$

This equation suggests to assume for the group k the following form o I:

$$I(m, \nu, \mu, t) = \alpha_k(m, t) I_P(T, \nu) + \mu \beta_k(m, t) \frac{1}{\theta(T, \rho, \nu)} \frac{\partial I_P}{\partial T} \tag{3.12}$$

α_k and β_k being the functions that describe completely the group. If there is LTE they take the values 1 and $-\partial_m T$, respectively; this makes it possible to manage correctly situations with one group only. On the other hand, when the system is far away from the equilibrium, in this case the accuracy can be reached only by taking a large number of groups. Let's write down useful properties for the operators 3.8, where $g = g(m, \nu, t)$:

$$L^k_+(g) = L^k_-(g) = \frac{1}{2} L^k(g); \tag{3.13a}$$

$$L^k_+(\mu g) = -L^k_-(\mu g) = \frac{1}{4}(\mu^k_a + \mu^k_b) L^k(g) \tag{3.13b}$$

$$L^k_+(\mu^2 g) = L^k_-(\mu^2 g) = \frac{1}{6}(\mu^{k^2}_a + \mu^k_a \mu^k_b + \mu^{k^2}_b) L^k(g) \tag{3.13c}$$

Therefore we can recast 3.9 as follows:

$$U_k = \frac{1}{c}\alpha_k L^k(I_P) \tag{3.14a}$$

$$S_k = \frac{\beta_k}{3}(\mu_a^{k^2} + \mu_a^k\mu_b^k + \mu_b^{k^2})L^k(\frac{1}{\theta}\frac{\partial I_P}{\partial T}) \tag{3.14b}$$

In order to get the group equations we are going to apply operators 3.8 using properties 3.13 to the equation 3.7 kwnowing 3.12:

$$\partial_m\left(\pm\frac{\mu_a^k+\mu_b^k}{4}\alpha_k L^k(I_P) + \frac{\mu_a^{k^2}+\mu_a^k\mu_b^k+\mu_b^{k^2}}{6}\beta_k L^k\left(\frac{1}{\theta}\frac{\partial I_P}{\partial T}\right)\right) = \\ + \frac{1}{2}L^k(\theta I_S) - \frac{\alpha_k}{2}L^k(\theta I_P) \mp \frac{\mu_a^k+\mu_b^k}{4}\beta_k L^k\left(\frac{\partial I_P}{\partial T}\right) \tag{3.15}$$

Now these equations are linearly combined adding and subtracting each other; after some algebra this result in:

$$\partial_m S_k(m,t) = c\theta_P^k(\rho,T)(U_{S,k}(\rho,T) - U_k(m,t)) \tag{3.16a}$$

$$\frac{\mu_a^{k^2}+\mu_a^k\mu_b^k+\mu_b^{k^2}}{3}c\partial_m U_k(m,t) = -\theta_R^k(\rho,T)S_k(m,t) \tag{3.16b}$$

Where $U_{S,k} = \epsilon_k(\rho,T)U_{P,k}(T)$ with $U_{P,k}$ being the Planckian energy density $U_{P,k}(T) = \frac{4\pi(\mu_b^k-\mu_a^k)}{c}\int_{\nu_a^k}^{\nu_b^k} I_P(T,\nu)d\nu$. The coefficients θ_P^k and θ_R^k are usually named Planck and Rosseland mean opacities and are defined as:

$$\theta_P^k = \frac{\int_{\nu_a^k}^{\nu_b^k}\theta I_P d\nu}{\int_{\nu_a^k}^{\nu_b^k} I_P d\nu} \tag{3.17a}$$

$$\theta_R^k = \frac{\int_{\nu_a^k}^{\nu_b^k}\frac{\partial I_P}{\partial T}d\nu}{\int_{\nu_a^k}^{\nu_b^k}\frac{\frac{\partial I_P}{\partial T}}{\theta}d\nu} \tag{3.17b}$$

Deviations from LTE conditions in the source function are taken into account by the

coefficients:

$$\epsilon_k = \frac{\int_{\nu_a^k}^{\nu_b^k} \theta I_S d\nu}{\int_{\nu_a^k}^{\nu_b^k} I_P \theta d\nu} \tag{3.18}$$

This is done in the approximation that $\epsilon(\rho, T)$ can be expressed as a function of the local density, temperature and material species alone. In practice, one may use some interpolation between SAHA(LTE) and corona equilibrium. In LTE all the ϵ_k are equal to unity. Such coefficients has been provided in tabular form. As a final consideration on these coefficients we can mention their dependence on the density. They decrease as the density decreases. This means that we will expect to see the radiation contribution to the shock formation as less effective at low densities. In particular a part of the energy of the plasma is carried away by the radiation field. Which means that for materials like gold where the densities cannot be low enough and the effective Z is quite high in order to see any shock we need for high intensities.

3.2.1. Boundary conditions

As had been pointed out, every group is composed by photons traveling in two directions. Let us consider the partial energy densities U_k^+ and U_k^- of the photons traveling to the right and to the left, respectively, and also the corresponding energy fluxes S_k^+ and S_k^-. They are given by:

$$U_k^{\pm} = \frac{1}{c} L_{\pm}^k(I) = \frac{1}{2} U_k \pm \frac{\mu_a^k + \mu_b^k}{4 c g_k^2} S_k \tag{3.19a}$$

$$S_k^{\pm} = L_{\pm}^k(I) = \frac{1}{2} S_k \pm \frac{\mu_a^k + \mu_b^k}{4} c U_k \tag{3.19b}$$

Where $g_k^2 = \frac{{\mu_a^k}^2 + \mu_a^k \mu_b^k + {\mu_b^k}^2}{3}$. Multiplying by μ and carrying out the integration over frequencies between ν_a^k and ν_b^k and cosines between μ_a^k and μ_b^k result in :

$$S_k^+(m_L) = -\alpha_L S_k^-(m_L, t) \tag{3.20}$$

Taking into account the previous expression it becomes

$$S_k(m_L) = -\frac{\mu_a^k + \mu_b^k}{2} \left(\frac{1 - \alpha_k}{1 + \alpha_k} \right) c U_k(m_R, t) \tag{3.21a}$$

$$S_k(m_R) = \frac{\mu_a^k + \mu_b^k}{2}\left(\frac{1-\alpha_k}{1+\alpha_k}\right) cU_k(m_L, t) \tag{3.21b}$$

For what concerns the simulations I am going to perform in chapter 4 I am going to use the following BC:

$$S_k(m_L) = 0 \tag{3.22}$$

$$S_k(m_R) = I \times A \tag{3.23}$$

For each $k = 1, 2, 3....$ where:

- I is the laser intensity in $\frac{W}{cm^2}$;
- A is the laser spot on the target in cm^2.

In general the code allows for very complex situations where from the left and from the right there are different lasers. We also know that a laser is never exactly monochromatic (remember that the energy of a photon is directly connected to its wavelength). Its band will always exibits a non-zero thickness. MULTI-FM can handle these situations in general. For what concern the scope of my work I do not exploit this feature.

3.2.2. Equation Of State:EOS

"In the 90's the scientific community believed that material physics would became simple as density increased. The electrons would be strongly degenerate and tend toward constant density, and the ions would be isolated in their own spheres, not unlike the monads of Leibniz... Models coming from statistical mechanics based on the Helmholtz Free Energy, would work well. Such models actually fail at high enough density, they are *qualitatively* incorrect. They observed changes in material structure that were entirely unexpected, and that the transition to a liquid state occurred at very different temperatures than had been predicted. We came to understand what is happening qualitatively by means of advanced computer simulations." [2].

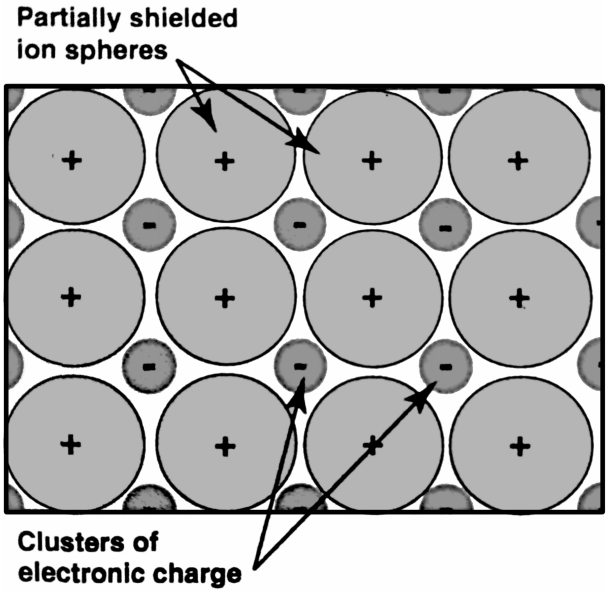

Figure 3.1: This is a graphical representation of the charge clustering, which is the phenomena behind the Fermi-degenerate state of matter [2].

Figure 3.1 illustrates the fundamental reason why unanticipated behavior arose. When spheres having the same dimension are used to fill a certain volume there will unavoidably remain unfilled regions between them. This model assumes that the electronic density is homogeneously constant over the whole ion clustering. What really happens is that electrons tend to cluster into the gaps among ions. This disuniformities of the electron density distributions makes the ions incompletely shielded ,and so they are affected each other ions too. This situation is the cause for the formation of chemical bonds, similarly to ionic bonds. The big difference respect to ionic bonds is due to the energies involved. In this case we are talking about transition energies in the KeV order while ionic bonds lies into the eV range. The theoretical approach provides two different ways to quantitavely descrive these interactions: The *Density Functional Theory* (DFT), a quantum-mechanical method which adopt special functions to describe the electron density, and the *Molecular Dynamics* (MD), which is a first principles based approach which make use of potentials to describe the forces acting among all the particles.These approaches are actually complementary since in some regimes it is necessary a quantum mechanical calculation in order to model the potentials ancting among all the ions.

In order to have a more realistic description one should take into account for the electronic bounds. Moreover, the transitions between different regimes should be approached carefully. In fact, high-density-matter very often evolves nearly to state of matter which are not high-density-matter, but solid or liquid. This complexity should be taken into

consideration once a computer simulation is performed. These difficulties make the problem a very complicated one. Theoretics approaches nowadays cannot withstand such a complexity. The use of a semi-empirical approach based on tabular Equation Of State is the best we can do. The idea is to perform a lot of experiments in order to have a big database for the thermodynamic variables (ρ ,p ,e ,T) for that specific materials under that specific irradiation conditions. By employing the aforementioned methods, such as DFT and MD, one can use a computer to numerically interpolate the data. The experimental device needed for performing EOS measurements is the so called Velocity Interferometer For Any Reflection (VISAR)(appendix B). The themodynamic consistency is a non trivial problem which arise once a numerical EOS is evaluated. Does the relation among all the thermodynamic variables respect the first law of thermodynamics? The only way to ensure this is to check it directly on the table. Landau and Lifšits in [35] showed that one can conveniently re-write the first law of thermodynamics as follows:

$$\frac{d(\rho e)}{dV} + p - T\left(\frac{dp}{T}\right) = 0 \tag{3.24}$$

Once the radiation field is taken into account in a tabular EOS the situation becomes even more problematic. Moreover, a characterization in terms of EOS do not exist yet for foams. This is a very important aspect since there is a lot of physics still to be developed about these promising materials.

3.3. Absorption process in a foam through effective models

Once the laser starts to ablate the foam target an expansion towards the laser generates a rarefaction wave. In the meanwhile the laser light is penetrating the target up to a distance defined by the concept of length of geometrical transparency $L_p(x,t)$. The evolution of this quantity is dictated by the homogenization process taking place during the irradiation due to which the pores initially fill with inhomogeneous plasmas. These plasmas mix into the pores leading, after the homogenization time t_h, to a homogeneous condition. Once the homogenization is completed the absorption is described through the inverse Bremsstrahlung mechanism. Longitudinal wave propagation predicts a compression after the rarefaction. This compression can be carried out by a shock wave if the conditions allow for the shock formation. There is a competition between the homogenization front propagation and the shock wave propagation. In [8] an evolution model for the length of geometrical transparency has been proposed. The absorption coefficient in a foam

$K_f(x,t)$ is defined as the inverse of the length of geometrical transparency:

$$K_f(x,t) = \frac{1}{L_p(x,t)} \tag{3.25}$$

Where L_p can be written as:

$$L_p(x,t) = L_{p0}\left(\frac{b_0}{\delta_0}\right)\left(\frac{\delta_0}{b(t)} - 1\right) \tag{3.26a}$$

$$L_{p0} \simeq \frac{\pi^2}{2}\frac{\rho_s}{\rho_p}b_0 \tag{3.26b}$$

- L_{p0} is the initial value of the length of geometrical transparency;
- $b_0$is the initial value of the solid element thickness(which has to be seen as a local clustering of atoms/nanoparticles);
- δ_0 is the initial value of the pore dimension(through the homogenization they will be filled with plasma);
- ρ_p is the average foam density;
- ρ_s is the initial solid element density.
- t_h is the homogenization time.

The evolution of the thickness of the solid elements in time can be expressed as:

$$\frac{db(t)}{dt} = \frac{\delta_0 - b_t}{t_h} \tag{3.27}$$

By solving the equation for $b(t)$ and recasting for K_f we get:

$$K_f(x,t) = \frac{\delta_0}{b_0 L_{p0}}\left(\frac{1}{\left(1 - \frac{\delta_0}{b_0}\right)(1 - H(x,t))}\right) \tag{3.28}$$

The quantity $H(x,t)$ is:

$$H(x,t) = 2\int_0^t \frac{dt'}{h_0(x,t')} \tag{3.29a}$$

$$h_0 \simeq 2.4 \times 10^{-3}\frac{Z^4\delta_0^2\rho_p}{A^{1/2}T^{5/2}} \tag{3.29b}$$

Quoting the work by Cipriani [8], $H(x,t)$ is the quantity to look at in order to properly

define the homogeneization degree into the foam. Now we can start to really appreciate the differences between the overcritical and the subcritical cases. It is a matter of defining a proper homogeneization criterion. In the sovracritical case we can say that a critical surface will for sure be fully developed with $L_p(x,t_h)=0$, which means $H(x,t_h)=1$. Here we have a singularity for the absorption model. In the subcritical case we can say that the length of geometrical transparency will not expected to be 0 at the homogeneization. In this case the proposed criterion states that the homogeneization can be considered as completed once is verified that the maximum plasma density is still below the average initial foam density. In this case $H(x,t_h)=1-\left[\frac{1-\left(\frac{\rho_p}{\rho_{crit}}\right)^{\alpha}}{1-\left(\frac{\rho_p}{\rho_s}\right)^{\alpha}}\right]^2$ where α is the so called fractal parameter we defined in 2.2. Experimental analysis tell us that in the subcritical case there are no the conditions for letting shock waves develop. In this case we talk about ionization waves.

3.4. IsFoam parameter as a measure of the homogenization degree

We can define the following parameter:

$$IsFoam(x,t)=1-\frac{H(x,t)}{H(x,t_h)} \tag{3.30}$$

So when $t=t_h$ the parameter $IsFoam=0$ stating that the target in x is no longer a foam since the homogeneization is completed there. For $t=0$ $IsFoam=1$. $IsFoam$ is therefore a measure of the homogeneization degree during the irradiation process. Thanks to this we can properly recast some of the equations written above. First of all, at the very beginning of the irradiation our absorption coefficient is given by:

$$K_f(x,0)=\frac{\delta_0}{b_0 L_{p0}}\left(\frac{1}{\left(1-\frac{\delta_0}{b_0}\right)(1-H(x,0))}\right) \tag{3.31}$$

Once the homogeneization is completed it is given by:

$$K_B=C\frac{1}{T^{\frac{3}{2}}}\left(\frac{\rho(t_h)}{\rho_{crit}}\right)^2\frac{1}{\sqrt{1-\frac{\rho(t_h)}{\rho_{crit}}}} \tag{3.32}$$

C is a constant defined in [28]. The problem is how to realize a proper transition between the two absorption models. Which is the absorption coefficients for $t>0$ and $t<t_h$?. In

[8] the following expression has been proposed:

$$K(x,t) = \sqrt{(K_f(x,t)IsFoam(x,t))^2 + (K_B(x,t)(1 - IsFoam(x,t)))^2} \tag{3.33}$$

Moreover, since the heat conduction is assumed to be entirely up to electrons it means that the effectiveness of this mechanism depends on the electron population, which in turn depends on the homogenization degree. Therefore we have to take it into account in our modelling. The equation for the heat conduction is then modified as follows, by introducing a dependence from the IsFoam parameter:

$$q(x,t) = -(1 - IsFoam(x,t))\chi_S \frac{\partial T}{\partial m} \tag{3.34}$$

Simulations performed in [8] have shown that in order to end up with correct result it is necessary to apply IsFoam to the momentum balance too:

$$\frac{\partial v}{\partial t} = -(1 - IsFoam(x,t))\frac{\partial (P_i + P_e + P_\nu)}{\partial m} \tag{3.35}$$

This has the effect of tuning the stresses on the fluid element considering the evolution of the material structure.

4 | Simulations performed with MULTI-FM 1D

In this chapter I am going to show the results about simulations performed with carbon and gold foams.The former is investigated for what concerns its potential use as ablator. In fact, most of recent important results coming from NIF are referred to High Density Carbon (HDC) ablators (diamond looks like the most promising bulk carbon version) in indirect schemes [3, 4]. The latter is not suitable as ablator. An high-Z target involves a strong radiation field able to reduce the energy available in the matter leading to weaker shocks. On the other hand there are studies which show how low-density gold foams can be used as hohlraum materials due to their higher efficiency in converting the laser energy into X-rays [32]. In the simulations, the thicknesses are taken larger than what they would be in the real applications. This is due to the fact that we are mainly interested in observing the physics of the whole process. In the next chapter I will show an optimized design for targets concerning both these applications. As written in the introduction of chapter 2 [12, 16], in a wide density range the behaviour of the hugoniot adiabat of porous substances is very similar to the behaviour of an ideal gas. This fact partially justifies the use of the EOS which has been adopted in this analysis: *Carbon as ideal gas* and *Gold as ideal gas*.

4.1. Analysis of the pressure levels in carbon planar targets

Carbon is one of the most promising materials for making ablators. In particular diamond(whose density is the bulk one) appears to be able to achieve higher yields. Proper diamond designs had the most calculated margin for achieving symmetry and the highest fuel absorbed energy, compared to plastic. I am going to start from the simulations of the laser interaction with the bulk homogeneous carbon. The tool at my disposal gives me the capability of simulating also lower densities carbon aggregates, eventually accounting for the internal structure too.The most important open points for what concerns the research

of innovative ablators are matter of compression efficiency/final pressure level and energy conversion efficiency of the laser light into mechanical energy transported through shock waves. MULTI-FM it's a 1D code but it can successfully used for the investigation of the aforementioned open points. As I stated in the title of this paragraph, the main quantity to look at is the pressure; nevertheless I am going to show also other quantities of interest in order to fully understand the physics behind the target ablation. The HDC results will be the starting point. The laser pulse shape adopted is a sin^2 function since this is the pulse shape of the ABC laser.

Table 4.1: High density carbon

Sim n.	EOS	thick[cm]	pore[μm]	av. ρ [g/cm^3]	Intensity [W/cm^2]
1	Carbon as ideal gas	0.015	none	3.53	10^{14}

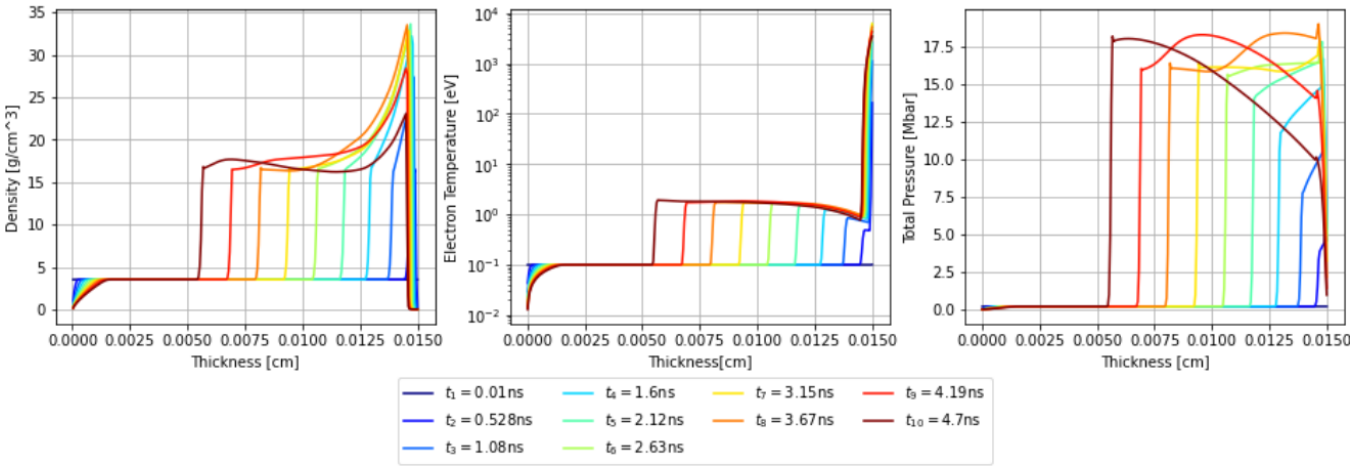

Figure 4.1: (a) Density evolution of the homogeneous bulk carbon target; (b) Electron temperature evolution of the homogeneous bulk target; (c) Pressure evolution of the homogeneous bulk carbon target.

As expected, when a HIL ablates an homogeneous target the shock is promptly formed, as shown in Fig.4.1.The initial curves exhibit higher density values respect to the final curves. This is in good agreement with the fact that at the beginning shock and thermal waves share the same spatial region. They will separate since they propagate with different velocities leading to a relaxed situation towards the end. Experimentally these velocities should slightly decrease with time due to the lateral spread of energy. In our 1D simulation this effect is not taken into account and in fact the velocities are almost constant.The temperature evolution ha been taken in log-y scale since in linear scale all the curves are superimposed at the surface of the target. This behaviour can be explained through the

following reasoning. In Section 3.3 the concept of length of geometrical transparency has been introduced. The bulk state density of the carbon is much higher than the critical density of the carbon (which by assuming ABC laser wavelength is 0.003 g/cm^3). In a material high density homogeneous material the critical surface, which is the surface at which the material become opaque to the laser light and so is reflected, is promply formed at the external target surface (length of geometrical transparency=0). This is the situation depicted in 4.1(b). The plasma is generated on the external surface of the target and the laser is not able to deeply penetrate. So the superficial temperature is much higher than the internal one during the whole laser pulse duration. In a foam the precence of pores allows for a non zero length of geometrical transparency which means that even in the overcritical case the critical surface is not promply formed(it takes time) and so the laser is able to penetrate the target up to a distance equale to the length of geometrical transparency. The pressure evolution follows the density profile:

$$\text{Pressure} \sim (\text{Temperature}) \times (\text{Density}) \tag{4.1}$$

This proportionality is what one could expects once the the ideal gas model is assumed. The simulations I am going to show have the aim of explaining the dependence of the pressure on both initial density and pore dimension. This is an important point and it is worth to recall that in these 1D simulations the most relevant quantity is the pressure. This quantity gives us the indication of how the use of a porous medium can help to enhance the compression of the target when used as an ablator. Now I am going to show simulations for three low-density carbon cases, the homogeneous case and two porous foam cases. This will also allow us to better understand the differences between simulations performed by properly taking into account for the internal structure and simulations for the homogeneous case. The easiest and more effective way is to show a realistic LDC case, coherently to the values achievable by the PLD technique 2.5.

Table 4.2: Carbon foam

Sim n.	EOS	thick[cm]	pore[μm]	av. ρ [g/cm^3]	Intensity [W/cm^2]
2	Carbon as ideal gas	0.1	1	0.05	10^{14}

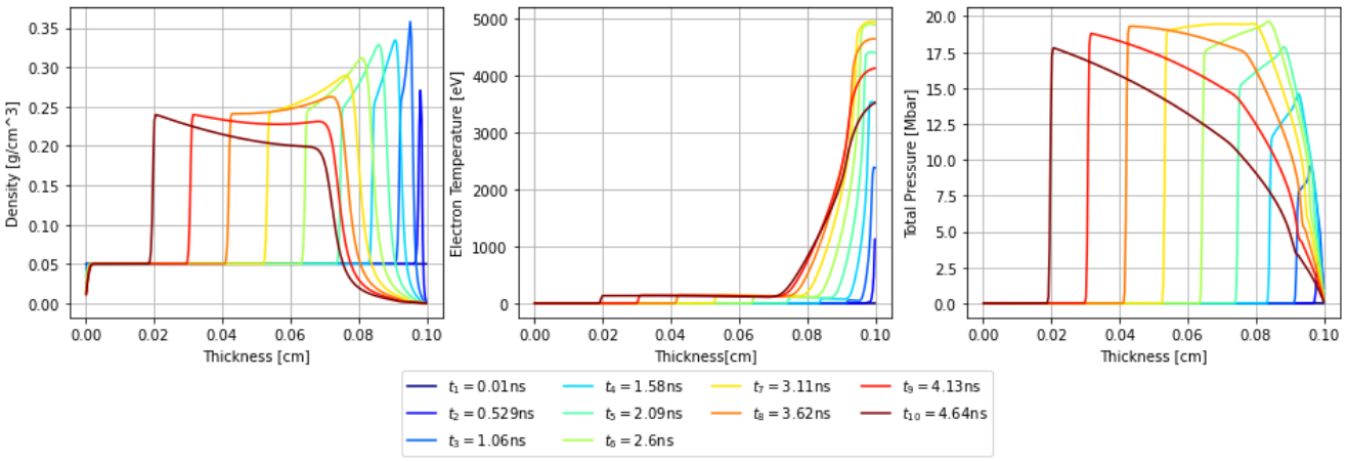

(a) Density evolution(homogeneous) (a); Electron temperature evolution (homogeneous) (b); Pressure evolution (homogeneous) (c).

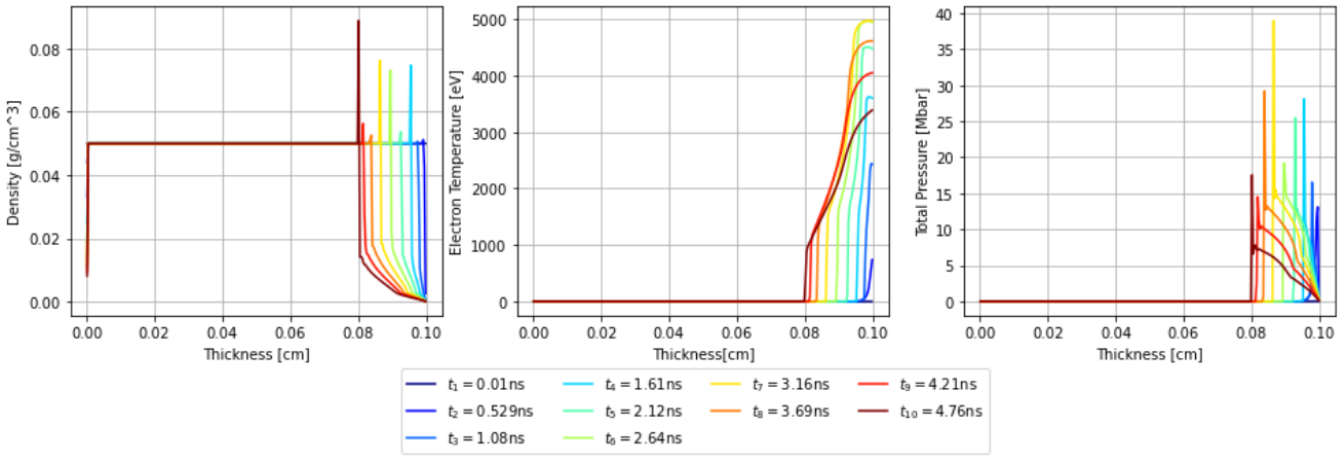

(b) Density evolution(foam)(a); Electron temperature evolution (foam) (b); Pressure evolution (foam) (c).

Figure 4.2

Starting from the density profile we can say that in the homogeneous case shon in Fig: 4.2.(a).(a), as expected, as in the bulk case the shock is promptly formed. This is an important point because I can state that the initial target's density does not play a role into the velocity of formation of the shock wave. The shapes of these shock waves are very similar to what is described in the book of Drake [2] (more precisely in *cap*.4, *par*.4.5). When the source of pressure ends (the laser pulse ends) a rarefaction wave (A.4) may propagate forward overtaking the shock. This is a Blast wave (A.5). In the foam case the shock formation takes significantly more time. The pore dimension is heavily involved into the velocity of formation of the shock wave. Moreover, the shock waves propagate slower with respect to the homogeneous case. In these Figures 4.2.(a).(a),4.2.(b).(a) we can qualitatively see how slower they are respect to the homogeneous case. The simulation

time has been setted to 5 ns in order to let the laser deposits all its energy and allowing the hydrodynamics to take place without increasing too much the computational time. As you can see, assuming the same thickness of the targets, at 5 ns the shock wave into the homogeneous target has traveled a larger distance with respect to that traveled into the foam. A similar comment can be done on the effect of the initial density on the shock propagation velocity. By comparing 4.2.(a).(a),4.2.(b).(a) we can say that the shock wave propagates much faster into the low density carbon target. In 4.2.(b).(a) oscillations in the density profile can be observed. They are related to numerical fluactuations which are due to the much lower thickness of the show front into the foam. As explained in Sec. 3.4 momentum balance and electronic heat transport equations must be modified by multiplying them by the factor $(1 - IsFoam)$, because the low availability of electrons in the partially filled pores limits the thermal conductivity, while the inhomogeneities in the density due to the pore filling process limit the mechanical response of the plasma to pressure gradients. One of the most important and evident effects of this tuning operation is the change in the shock front thickness, which is lower in the foam compared to the homogeneous medium. MULTI-FM makes spatial discretization of the x-axis into cells. The shock fronts observed into the foam are so tight that the wave is fully contained by 2-3 cells. While moving from one time step to the next, the shock front moves across the numerical cells, which may have (and this is generally the case) different values of the IsFoam parameter, and in turn of the limiters. This fact creates a numerical fluctuation which slightly changes the maximum values attained by the quantities at the shock front. This does not happen in the homogeneous case, where the shock front is larger and the properties of the medium in terms of conductivity and hydrodynamics are the same in the whole computational domain. For what concerns the temperatures there are several observations which can be done. The heat transport is related to the electronic populations. This means that increasing the density of the material leads to an increase of the electron population, and therefore to a faster propagation of the heatwave. Therefore we expect a slow down of the thermal heat wave when the density is reduced. We also expect a reduction of the heatwave speed with increasing the pore size, due to the larger homogenization time. We do not observe any difference in the absolute value of the temperature peak by increasing the pore dimension. We actually observe that the absolute temperature peak decreases as the initial density density does. For what concerns the pressure, in the homogeneous Low Density Carbon (LDC) case the pressure levels are quite similar to those of the homogeneous HDC case (which is reasonable since the temperature in the homogeneous case is higher but density in the LDC case is smaller, see eq. 4.1). In a foam the pressure level is expected to be higher [11], and in fact this is what we can see here. This is in agreement with what has been said in Section 2.3 about the role of

pores in the pressure development: larger pores correspond to higher pressure. However, even smaller pores, as the ones considered here, lead to a higher pressure, compared to the homogeneous medium. To support this statement, I will now show the results of the simulations of foams with increasing pore size up to 10 μm.

Table 4.3: Carbon foam

Sim n.	EOS	thick[cm]	pore[μm]	av. ρ [g/cm^3]	Intensity [W/cm^2]
3	Carbon as ideal gas	0.1	10	0.05	10^{14}

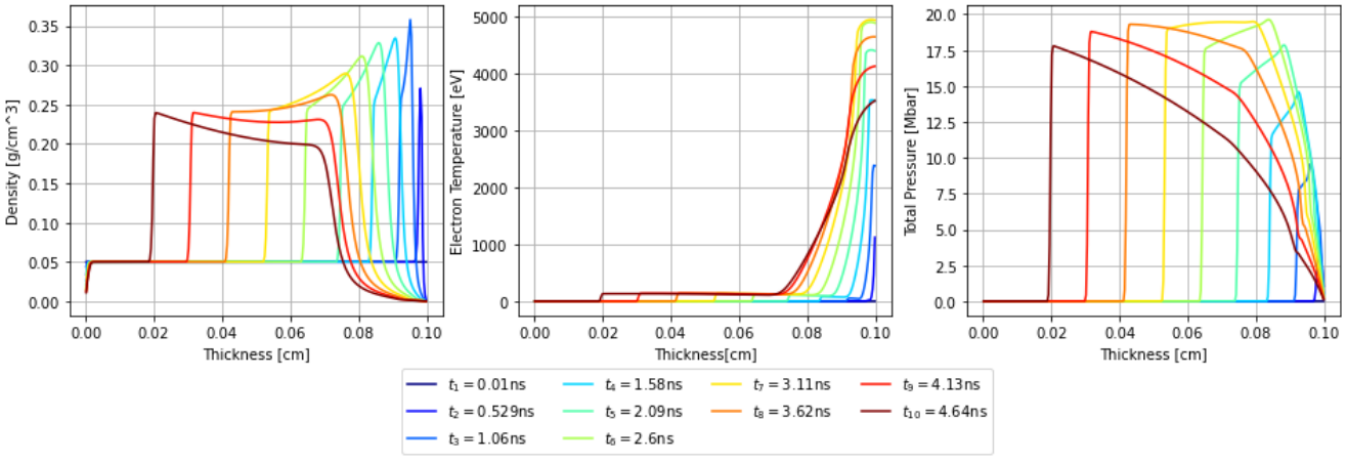

(a) Density evolution(homogeneous) (a); Electron temperature evolution (homogeneous) (b); Pressure evolution (homogeneous) (c).

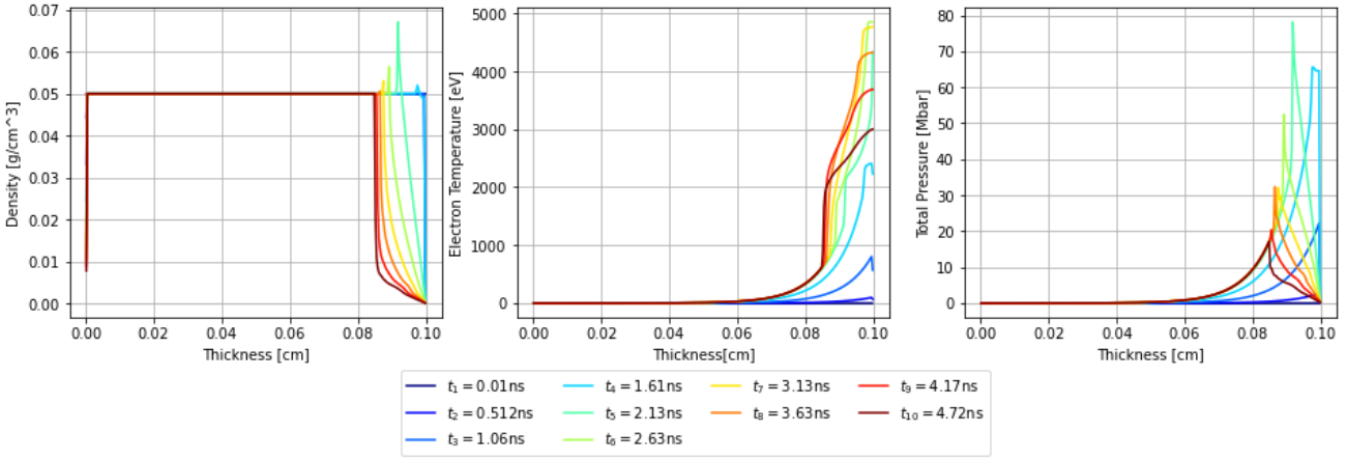

(b) Density evolution(foam) (a); Electron temperature evolution (foam) (b); Pressure evolution (foam) (c).

Figure 4.3

The shock wave propagation velocity depends on the pore dimension as can be seen by the comparison of 4.2.(b).(a) and 4.3.(b).(a).The bigger the pores the slower the shock

propagation. Moreover, the pore dimension heavily affects the final pressure levels. A 10 μm pore foam lies in the group of big pore foams.This pore dimension range, from 1 to 10 μm, is believed to be the most realistic one once the PLD is considered as foam production technique. What can be seen in the foam temperature profile 4.3.(b).(b) is the effect of the length of geometrical transparency 3.3. The bigger the pores the bigger the distance that the laser pulse is able to travel into the target even before the homogeneization. In a small pore foam this effect is much less pronounced 4.2.(b).(b).

4.2. Efficiency of absorption in carbon targets

In this section I am going to show which is the trend of the absorbed energy by changing the target thickness.

Table 4.4: HDC

Thickness[cm]	0.005	0.01	0.03	0.05	0.1
Abs.eff.	0.966	0.975	0.98	0.996	1

Table 4.5: LDC

Thickness[cm]	0.005	0.01	0.03	0.05	0.1
Abs.eff.	0.44	0.822	0.84	0.926	0.936

Table 4.6: 1 μm pore carbon foam

Thickness[cm]	0.005	0.01	0.03	0.05	0.1
Abs.eff.	0.59	0.918	0.922	0.926	0.940

Table 4.7: 10 μm pore carbon foam

Thickness[cm]	0.005	0.01	0.03	0.05	0.1
Abs.eff.	0.576	0.874	0.956	0.964	0.970

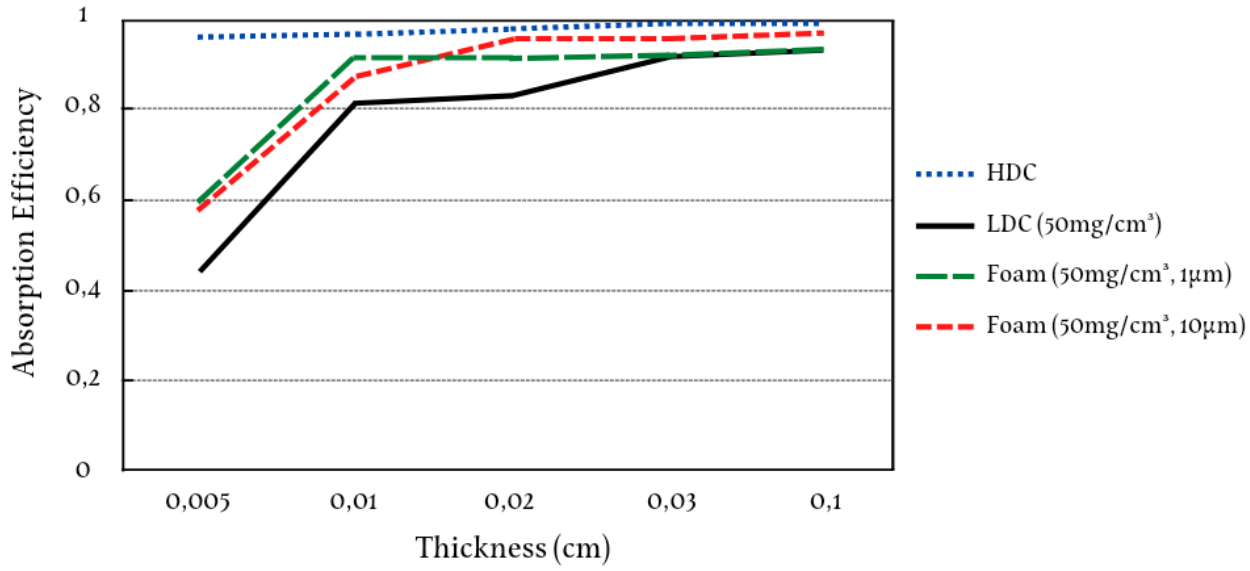

Figure 4.4: Absorption efficiency for different target as a function of the thickness.

As can be seen in Fig. 4.4, the HDC absorption profile is almost constant by changing the thickness by order of magnitudes. I the other cases, we can observe a dramatic change from 0.005 cm to 0.01 cm, which is in good agreement with the fact that the target is expected to be completely ablated before the full laser deposition. Moreover this is mitigated by using foams, and also this effect is shown on the graph. The foam case with 10 μ m pores is the one which exhibits the highest variation. For low values of the thickness(from $50\mu m$ to $100\mu m$) its capability to absorb energy is lower than the $1\mu m$ pore case.This is due to the fact that the initial transparency length of the foam is larger than the target thickness. From 300 μ m on the foam with 10 μm pores has the closer absorption efficiency to the HDC case. The homogeneous LDC case exhibits the lowest energy absorption for all thicknesses. Nevertheless let us observe that from 500 μ m on it is almost indistinguishable from the case of the foam with 1 μ m pores . This effect is reasonable since for that values of the thickness a 1μ m foam is very similar

to an homogeneous material. This evaluation confirms the fact that foams have an high capability for energy absorption. At $100\mu m$ thickness the HDC absorb $97.5J$, the LDC foam($10\mu mpores$) target absorb $95.6J$, but the density of the former is about 70 times higher than that of the latter. As you can see in all the analyzed cases I get the plateau for absorption.

This is in contrast with what we already know about low-Z foams. Experimental evidences [11] show that a foam is more efficient with respect to an homogeneous medium once the plateau region is achieved. The bigger the pores the higher the efficiency.This is related to the reflection model implemented in MULTI-FM. Laser light while penetrating the target is partially reflected. This reflected light is not completely lost by the target. In a foam this effect is enhnanced by the microstructure. Pores are able to partially trap reflected light, leading to an higher absorption efficiency.This has been experimentally proven in [10] and compared with a simple model. However, this aspect does not invalidate the previous results about carbon since I got higher pressure levels in the foam case despite the lower absorption efficiency.

4.3. Summing up about carbon

The results obtained for the bulk homogeneous carbon tell us that this material is for sure of interest as ablator. My simulations show that higher pressure levels can be achieved though the use of foams, as expected [8]. The internal structure of these foams is a very important aspect and to the best of my knowledge there are no available articles in the literature devoted to it. Another potential advantage for using foams is due to the fact that, as shown in the simulations, blast waves (which are usually formed in homogeneous target irradiated by a High Intensity Laser) do not develop. By quoting the chapter 4 of the book of Drake [2] these blast waves are thought to be one of the causes for Rayleigh-Taylor instability. As written in [5] the risk for Rayleigh-Taylor is a real one. During the implosion, the ablation front is unstable to the R-T instability. Although the ablation process itself helps in stabilizing the front, it is calculated and observed that even microscopic defects on the capsule surface grow several hundreds of times. These defects are another source for this instability. The preheat, which could lead to a mixing of the ablator and the cold fuel into the hotspot, is another cause for R-T. The use of foams is not a complete solution but it could be really useful since one of the main causes is reduced.

4.4. Analysis of the radiative heat waves in gold planar targets

As anticipated in chapter 2, section 2.4, a gold foam is a promising alternative as a constituent material of the hohlraum. A few works are available studying the effect of the radiation on shockwaves in gold foams, but in these works the internal structure is not considered and modeled[32]. I will show the results of the quoted article and then I will compare them with simulations I performed under the same conditions; then I will discuss what happens without neglecting the internal structure. In these simulations, the pulse shape is a step function (FWHM=1 ns) having a rising/decreasing time of 100 ps, with an intensity of 5×10^{14} W/cm^2. All the curves I am going to show are taken at 0.4 ns as in [32]. The EOS I use is taken from the SESAME database which is the same database to adopted in [32], so very likely the two EOS corresponds. With the following simulations, I want to show the conditions for the transition of the radiation heatwave from a supersonic to a subsonic regime as the foam density is increased. The aim of this section is to show the similarities in between their results and mine. To do so the criterion I have choosen is to verify the conditions for having a supersonical radiative heat wave.(perché me l'aveva segnalata? chiedere) To do so we have to compare the radiation temperature profile and the density profile. The density profile give us the information about the shock velocity, which is of the order of the sound speed. The radiation temperature profile, which represents the temperature of the plasma once black body radiation is assumed, gives us the information about the position of the radiative heat wave. If the radiative heat wave is developed slower or at the same rate as the shock wave we talk about *"subsonic radiative regime"*. If the radiative heat wave is developed faster than the shock wave we talk about *"supersonic radiative regime"*.The simulations are performed with the MULTI-FM code.

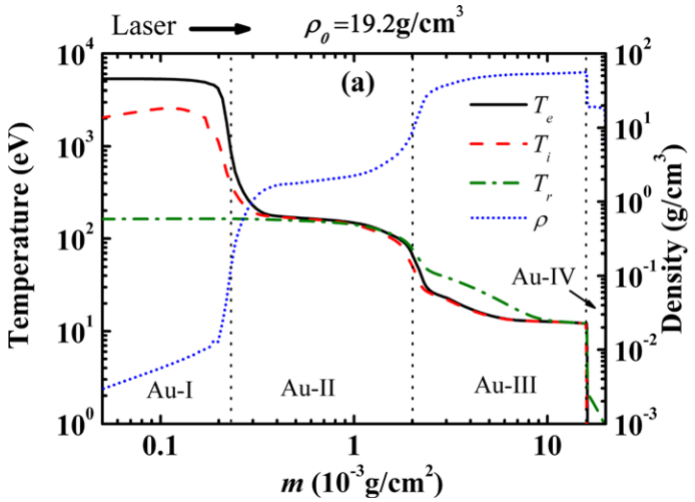

(a) Simulation of the electron, ion and radiation temperatures and density of a solid gold target [32]. The laser comes from the left. The plot is referred to the Lagrangian coordinate m.

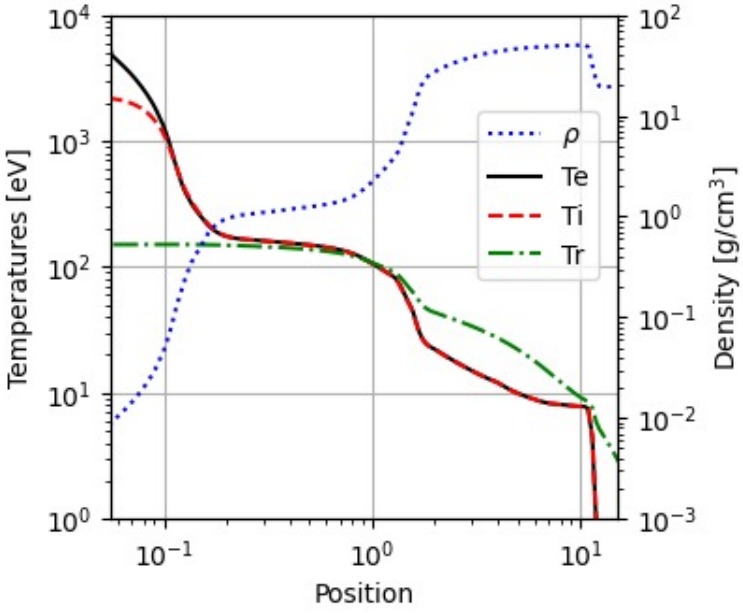

(b) Simulation of the electron, ion and radiation temperatures and density of a solid gold target I performed with the version of MULTI-FM at my disposal. The laser comes from the left. The plot is referred to the Lagrangian coordinate m.

Figure 4.5

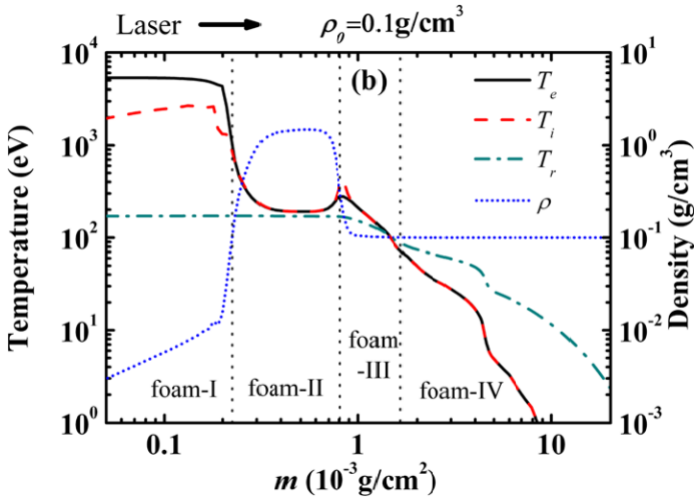

(a) Simulation of the electron, ion and radiation temperatures and density of a homogeneous LDG target [32]. The laser comes from the left. The plot is referred to the Lagrangian coordinate m.

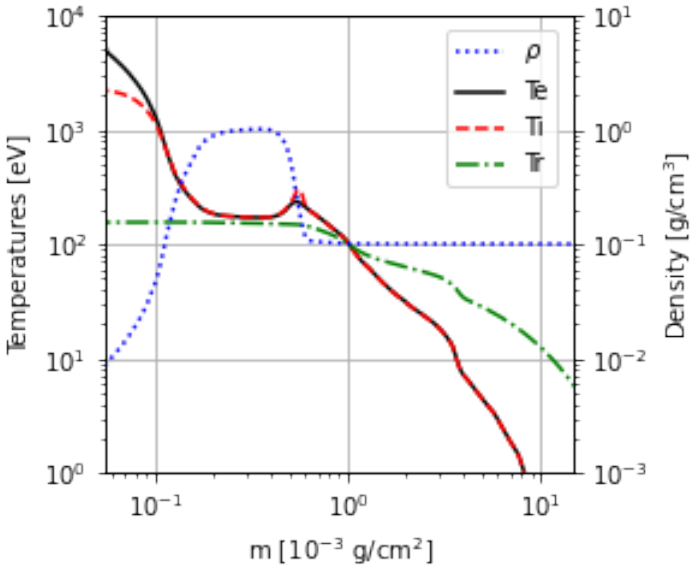

(b) Simulation of the electron, ion and radiation temperatures and density of LDG target I performed with the version of MULTI-FM at my disposal. The laser comes from the left. The plot is referred to the Lagrangian coordinate m.

Figure 4.6

In 4.5(a) the density profile indicates that the shock wave develops together with the radiative heat wave, as indicated by the radiative temperature profile. Therefore, the radiative heat wave is subsonic in this case. In 4.5(b) is shown my simulation for the

bulk gold case, under the very same irradiation conditions. The two profiles evolve quite similarly. Both of them show a subsonic/sonic radiative heat wave. The differences between these simulations are due the EOS and the opacities. For what concerns the latter, in [32] there are no available informations about the models they adopted. Once the density is lowered to the one of the homogeneous gold foam the case of an homogeneous LDG target the situation changes. In 4.6a is shown that the radiative heat wave front progapates faster than the shock wave, meaning that the radiative wave is supersonic. In the LDG target my simulation 4.6(b) predicts a much less pronounced shock respect to what is seen in 4.6(a) and a supersonic radiative heat wave regime is enstablished too. So my simulations are in agreement with the simulations showed in [32] with respect to the choosen comparison criterion. Let us consider, for example, figure 4.5(a). Four plasma zones can be identified [32]. The first one is related to the laser deposition/thermal conduction. The second one is the reemission zone where the plasma emits most of the radiation. The third one is the shock formation zone. The fourth one is the undisturbed zone. Now I am going to show the simulation which is missing in [32], the one which takes into account for the internal fractal-like structure of the gold foam.

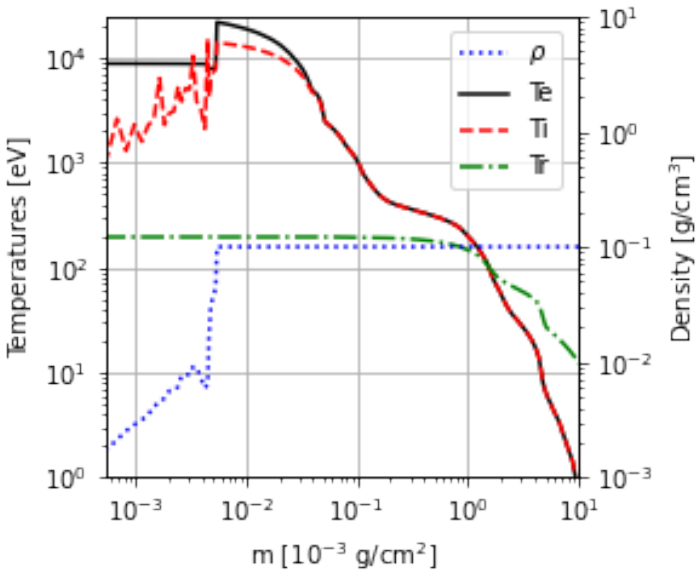

Figure 4.7: Gold foam target. Pore dimension 1 μm.

This is the result of my simulation about a foam target taking into account for internal structure, assuming 1 μm as pores dimension. A mechanical wave is early developed and then the profile is completely flat . Comparing with the previous situations depicted in Fig. 4.5 and 4.6, the final density is much lower. In these conditions, having a strong radiation field in comparison to low-Z materials, the mechanical wave development into

the target seems to be suppressed. The radiation field which is enstablished due to the laser matter interaction sees the target as subcritical even if the foam average density assumed (100 g/cm^3 is much higher than the critical density (17 g/cm^3), which means that it is able to deeply penetrate the target (this is an effect related to the length of geometrical transparency). The radiative heat have is supersonic and heats the target in depth before it is able to fully develop hydrodynamics and therefore mechanical waves. All the energy deposited by the laser is transported through this mechanism.

4.5. Summing up about gold

The results of this analysis are quite promising. The fact that my simulations are not completely fitting those reported in [32] is due to the differences in the tables for EOS and opacities used in the two cases. In the low density homogeneous gold case we can see that a mechanical wave is generated, but it is not comparable to the one generated in the bulk case. In the foam case (low density porous material), which is not present in [32], mechanical waves are not developed at all. This means that very likely the reemission zone (which is the one associated to the X-ray emission) is way much bigger respect to the bulk gold case and incorporates the shock formation zone. This fact, if validated by experiments, would imply that microstructured gold foams could represents the next generation of hohlraums being much more efficient in converting the laser energy in X-rays.

5 | Design of optimized foam targets for experiments at the ABC facility

In this chapter the focus will be on the design of optimized targets for laser-foam interaction experiments. The theoretical work carried out in chapter 4 represents the starting point of this discussion. The information that I got from the simulations will be exploited in order to determine, through further simulations, the set of optimized parameters which lead to the ottemperation of the purpose. For what concerns the carbon foam target which I am investigating as ablator, its purpose is to convert as much laser energy as possible into mechanical energy.To do so, the target has to withstand the full laser pulse while maximizing the final pressure. For what concerns the gold foam target which I am investigating as hohlraum, its purpose is to convert as much laser energy as possible into X-rays. To do so, the target has to withstand the full laser pulse while suppressing the development of mechanical waves. As final effort I will present the methodologies and the diagnostics which would be involved for the validation of the design I am proposing.

5.1. Design of an optimized planar carbon target

The simulations I carried out in Chapter 4 tell us that carbon foams have the potentiality to be better ablators respect to a HDC one and give the indications for designing a realistic planar foam target made with carbon. The aim of this section is, through additional simulations, to show which are the parameters which better satisfy the criterion pointed out above, so the capability of the target of absorbing all the laser energy while maximizing the final pressure. Let me start talking about the equation of state adopted. I will again assume, as in chapter 4, the ideal gas model for connecting the thermodynamic variables of the target. This is justified since previous experiments on plastic foam targets [12, 16] have shown that the hugoniot curves (Appendix A.1) of a material in the form of a foam and in the form of ideal gas are very similar over a wide range of densities. It is

worth to be noted that nowadays there are no available experiments conducted for the EOS measurement of a whatever realized foam-like material. For what concerns laser parameters, the waveform, the wavelength, the FWHM, the duration and the focal spot are characteristic of the ABC laser (Sec. 1.4). The other parameters over which I have control are: target thickness, pore dimension, average initial density, laser intensity.
The target thickness have to be enough to sustain the full laser deposition. If the target would destroyed prior the full deposition there would be a non optimal conversion of the laser energy into mechanical energy. Moreover a portion of the laser would preheat the fuel leading to a non adiabatic compression. If is taken too big the shock waves would relax leading to a lower final pressure applied at the target's end.
The pore dimension plays an important role on the achievable pressure.As shown in Sec. 4.1 the bigger the pore the higher the final pressure.
The average initial density has to be high enough in order to allow the target to be overcritical respect to the wavelength of the laser beam. As explained in Sec. 3.3, this is a necessary condition for the shock formation.
The laser intensity have to lie in a useful range for ICF purposes, so 10^{13-15}W/cm^2. In this range both electrons and ions can actively partecipate to the hydrodynamic of the pellet implosion.
All these parameters influence each other and of course this will heavily affect the final outcome. Thanks to the knowledge of the involved phenomena, I can define an initial set of parameters which I believe to be already good for achieving the purpose. Then, in order to optimized them, I carried out a heavy simulative work through properly tuning the initial values of the parameters. In Table 5.1 the are showed the values of the initial parameters of the non optimized planar ablator. In Figure 5.1 are shown the profiles of density, temperature and pressure into this target.

Table 5.1: Non optimized carbon foam target

EOS	thick[cm]	pore[μm]	av. ρ [g/cm^3]	Intensity [W/cm^2]
Carbon as ideal gas	0.005	1	0.05	10^{14}

Table 5.1: Radiation off

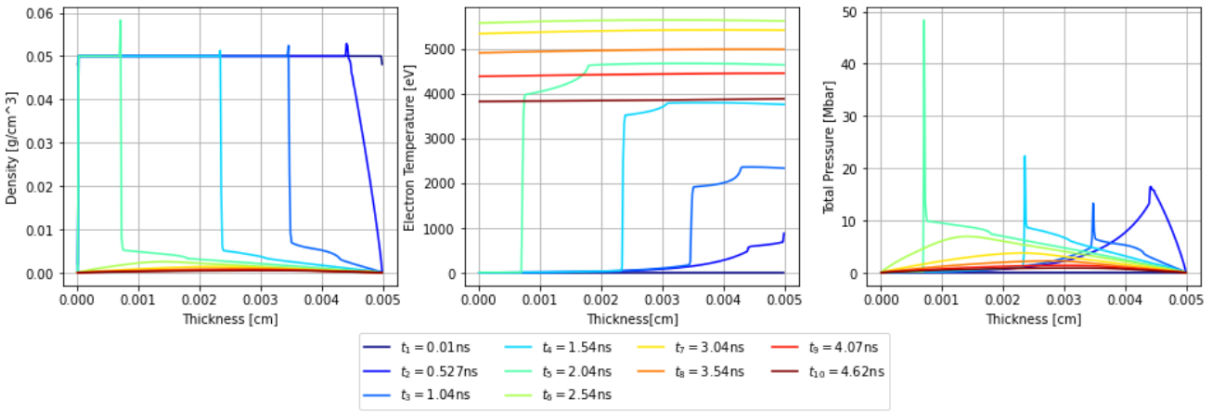

Figure 5.1: Density, electron temperature and pressure evolution of the non optimized carbon foam target under irradiation.

In all the plots can be observed that this target is not able to withstand the full laser pulse. From about 2.5 ns on concave curves takes place which meas that the target is completely ablated. Increasing the target thickness alone is not a solution. In fact this would relax the shock waves, decreasing the pressure. Moreover we know that the ablator's thickness have to not exceed 200 μm, in order to be coherent to what is expected to be a good aspect ratio for the fuel pellet [36]. What realizes the final optimized configuration is the knowledge of what happens by varying a parameter and its interaction with the others. I performed simulations accounting for all the aforementioned effects. In Table 5.2 the optimized parameters are reported.

Table 5.2: Optimized carbon foam target

EOS	thick[cm]	pore[μm]	av. ρ [g/cm^3]	Intensity [W/cm^2]
Carbon as ideal gas	0.01	10	0.06	6×10^{13}

Table 5.2: Radiation off

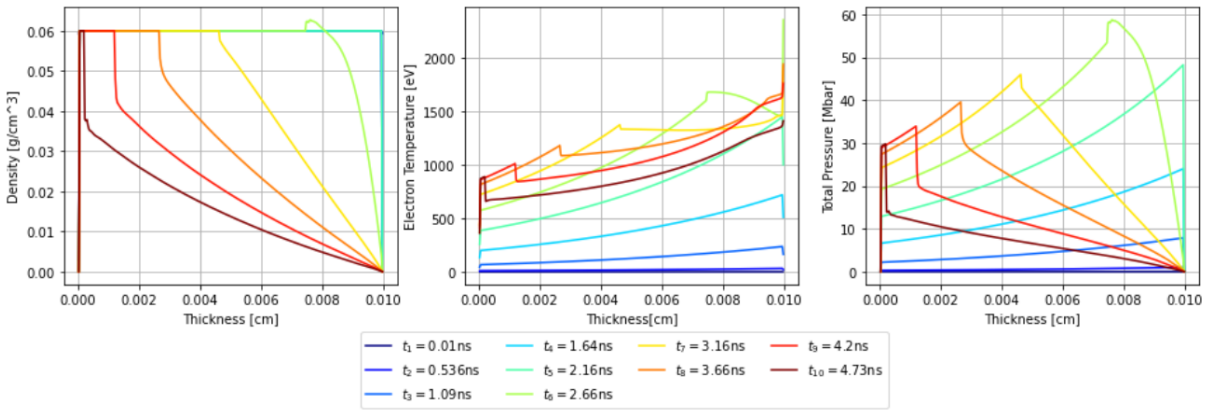

Figure 5.2: Density, electron temperature and pressure evolution of the optimized carbon foam target under irradiation.

In Figure 5.2 are shown the profiles of density, electron temperature and pressure of the optimized carbon foam target under irradiation. The target now is able to withstand the full laser deposition. The final pressure in Fig. 5.1 ,prior the complete target ablation, is actually higher than the final value observed in Fig. 5.2. This may be missleading but as stated above there must be the simultaneous fullfilment of two requirements: the target must withstand the full laser deposition while maximizing the final pressure. As additional consideration let me point out that the design in Table 5.2 avoids shock relaxation since the target at the end of the irradiation is almost completely consumed.The optimized design I proposed is able to fullfill all the listed requirements. As final comparison I want to show what happens in a high density carbon target assuming the same parameters shown in Table 5.2, except for the pore dimension since it is homogeneous. In Fig. 5.3 are shown the density, electron temperature and pressure of the HDC target under the same irradiation conditions of the optimized foam target case. The final pressure achieved in this case is more than 4 times lower than the final pressure achieved in 5.2.

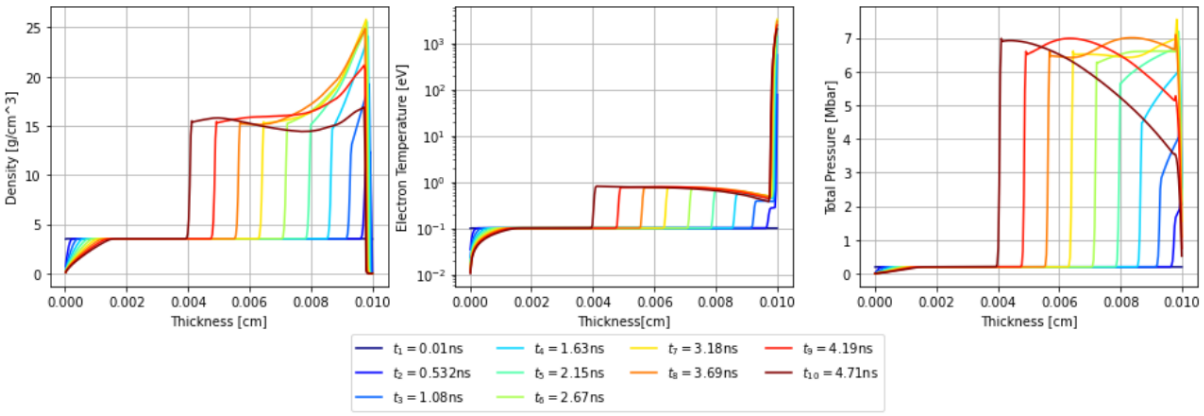

Figure 5.3: Density, electron temperature and pressure evolution of a HDC target under irradiation. Temperature is taken in semilog-y scale for the reason explained in Sec.4.1

To conclude the carbon target design there are two aspect left. First of all, the optimization has been carried out for a target intended for the direct ablation. The ABC laser beam has a wavelength of 1054 nm (Section 1.4). The electron critical density associated to such a wavelength is in the order of 3×10^{21}electrons/cm^3 while the electron density of a 60 mg/cm^3 carbon target is in the order of 18×10^{21}electrons/cm^3. So, as required for the formation of a shock wave (section 3.3), the average density of the optimized foam target is overcritical in relation to a 1054 nm laser beam. What if the wavelength in play of the laser ligth would be close to the characteristic wavelength range of X-rays (So in the order of 1 nm as upper value)? In that case our target would be subcritical respect to the incident light and there would not be the conditions for the shock formation. In an indirect configuration the ablator would be irradiated by X-rays, therefore the target parameters listed above would not be adequate.
Finally, I want to consider the production technique too. In Section 2.5 the Pulsed Laser Deposition has been presented. I explained the main differences between the ns-PLD and the fs-PLD. The achievable densities are quite similar therefore it will not represent one of the selection criterions. Carbon is one of the few materials which do not exhibit a liquid phase. This is very important since this is believed to be the reason why onto the substrate there are no microscopic carbon droplets deposited (which are deleterial for the foam aggregation). For carbon, ns-PLD and fs-PLD behaves very similarly while for other materials (such as gold) it is not the case. One of the most important difference between PLD deposition regimes is that in the ns-PLD there is the built up of a single aggregates population, while two aggregates populations are observed in the fs-PLD. So a foam deposited with fs-PLD will exhibits non uniformities at the nanometric scale. The implosion symmetry is very sensitive to the presence of microscopic defects on the ablator surface.

There are no available studies devoted in the investigation of the influence of nanometric structural disuniformities on the hydrodynamics development of the shock waves into the ablator. For the time being there are no foreseeable issues in adopting a ns-PLD while there may be an implosion asymmetry due to the use of a fs-PLD. Therefore the carbon foam target should be realized through a ns-PLD.

5.1.1. How to measure the pressure level

The measure of the pressure level at the end of a shock wave is not a straightforward task. Nevertheless, as I am going to explain, at the ABC facility the available diagnostics allow for two possible approaches. Let me point out the experimental conditions first.
The carbon foams parameteres are reported in Tables 5.1 and 5.2. The ABC experimental chamber operates at a BKG pressure in the order of 5×10^{-4} Pa. The ABC laser characteristics are those reported in Sec. 1.4 assuming the intensity reported in Table 5.2.

For what concerns the experimental techniques let me start presenting the Impedance Matching, which allows for a measure of the breakout pressure. The breakout pressure is the pressure associated to the shock wave as emerging from the target surface.

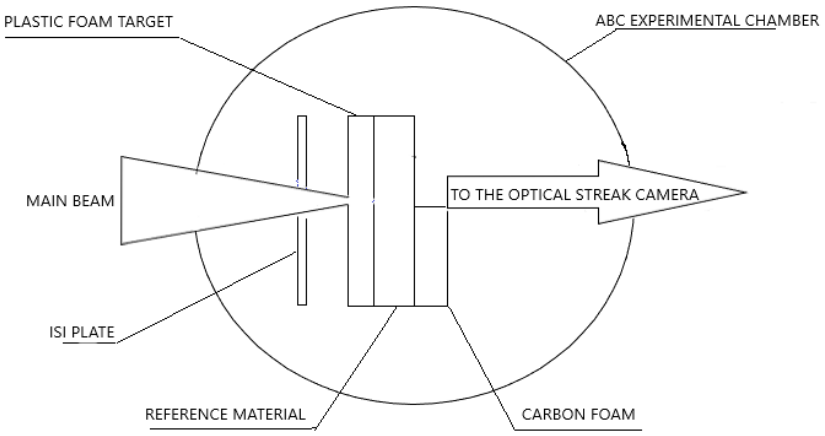

Figure 5.4: Experimental set-up for the breakout pressure measurement through impedance matching.

Into the experimental chamber we have:

- Induced Space Incoherence Plate (ISIP), whose aim is to smooth the laser beam for ensuring a more planar shock, which is important for having a precise measure of the breakout times;

- Plastic foam target, whose aim is to generate a strong planar shock which will propagate into the reference target having a negligible X-rays production;
- Reference target, which must be a well chatecterized target in terms of hugoniot adiabat and equation of state;
- Carbon foam target, which is the object of the measurement.

Though the knowledge of the entrance and breakout times of the shock into the reference target and the carbon foam, which are measured by the optical streak camera, we can recast the shock propagation velocity in both the targets knowing the their thickness. Since the reference material is chosen to be very well characterized we know which are the values of the particles velocity and the pressure at the interface. As explained in Ref. [33], at the interface the particles velocity and the pressure is conserved. We take advantage on this obtaining the breakout pressure of the carbon foam target.

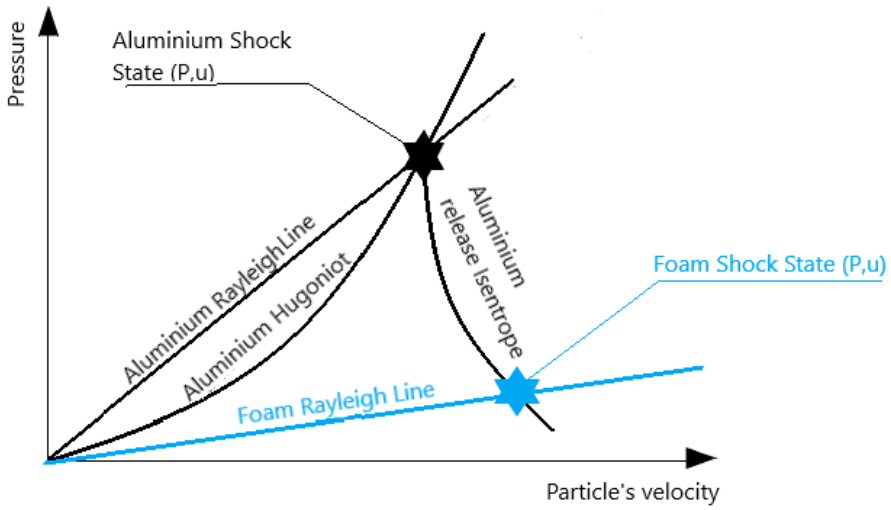

Figure 5.5: Impedance matching graphycally shown on the $P-u$ plane. Here as reference material Aluminium is adopted.

In Fig. 5.5 is shown the method which allows to determine the foam shock state at the target surface. The Rayleigh lines are straight lines defined on the $P-u$ plane, where u is the particle velocity, by the relation:

$$P = U_s u / V_0 \tag{5.1}$$

Where:

- P is the pressure;
- U_s is the shock velocity;
- V_0 is the target specific volume;
- u is the particle velocity.

The Rayleigh lines of the two materials are known once the shock velocities are measured by the streak cameras. The Hugoniot curve (Sec. A.1) of the reference materials, which is well known, is translated by means of the equation the Rankine-Hugoniot conditions (see Ref. [33]) from the $P - V$ plane to the $P - u$ plane. Once the shock wave arrives to the rear side of the reference material a rarefaction wave, which in Fig. 5.5 is called release isentrope, is generated. The intersection between the Rayleigh line of the carbon foam and the rarefaction wave of the reference materials on the $P - u$ plane give us the foam shock state.

On the other hand if we want to compare the efficiency of two different ablators of converting the laser energy into mechanical energy, the so called ablation loading, we can adopt another technique as shown in Ref. [11]. The technique consists in measuring the crater volume, generated by the shock wave as emerging from the carbon foam, onto a proper substrate positioned on the rear side of the ablated foam. In the reference article [11] an experimental campaign has been conducted at the ABC facility for the evaluation of the ablation loading for different plastic foams target. In order to use this method for comparing the ablation loading of different carbon foam target the experimental set-up will be the very same.

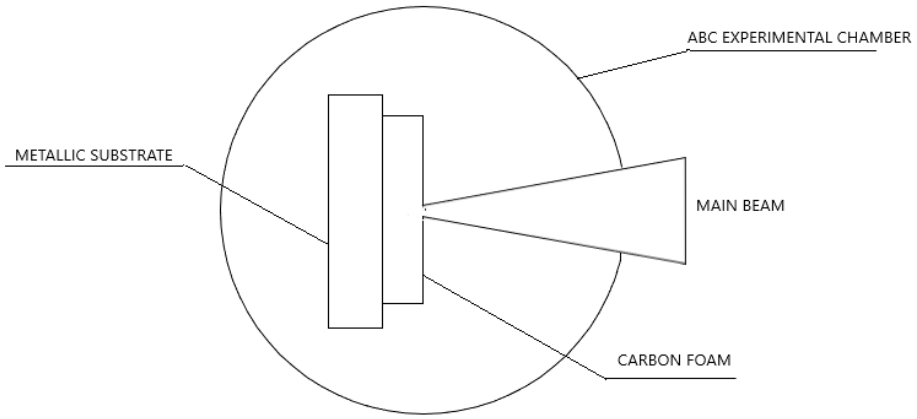

Figure 5.6: Experimental set-up for the ablation loading measurement.

For what concerns the substrate, in the reference article [11] an aluminum target is adopted

whose thickness is taken to withstand the full ablation loading.

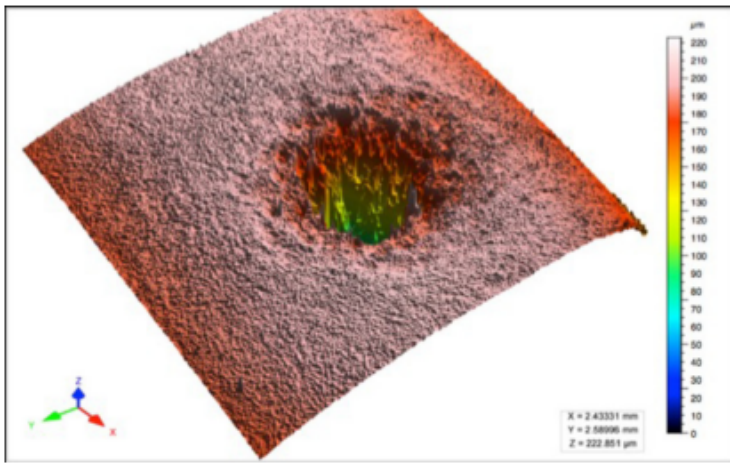

Figure 5.7: Visualization of a typical crater on a alluminium substrate [11].

By comparing the craters volume one can retrive which ablator exhibits the highest ablation loading. Figure 5.7 has been retrived through a confocal microscope. It is worth to be noted that there is no available literature about the use of this technique for carbon foam targets. The targets employed in [11] are micro-structured plastic foams.

5.2. Design of an optimized planar gold target

As explained in Sec. 5.1, also in this section I will take advantage on the theoretical work I carried out in Chapter 4. My results shown that gold foams, once ablated by a high intensity laser, exhibit a higher suppression of the mechanical waves respect to a High Density Gold (HDG) target. As a matter of energy conservation the laser energy which is not absorbed by the shock wave development may be involved into the X-Rays generation. The hohlraum has to maximize the conversion of the laser energy into X-Rays. Performing additional simulations respect to those showed in chapter 4, my aim is to define the target parameters which better satisfy the aforementioned requirement. Let me start again talking about the equation of state adopted. Same considerations listed in Sec. 5.1 for what concerns the adoption of the ideal gas model. For what concerns laser parameters, the waveform, the wavelength, the FWHM, the duration and the focal spot I refer to Sec. 1.4. The other parameters over which I have control are: target thickness, pore dimension, average initial density, laser intensity.
The target thickness have to be enough to sustain the full laser deposition. The precence of the pores is a crucial aspect since, as shown in Section 4.4, there is a dramatic change

passing from the LDG case to the foam gold case. In fact once the pores are properly accounted there is a huge suppression of the mechanical waves.
For what concerns the role of both pore dimension and initial average density a further investigation is required due to the complexity introduced by the radiation field. In fact, MULTI-FM 1D has been validated by ablation experiments only for low-Z materials, therefore in those cases in which the self-generated radiation field can be neglected. Therefore both the pore dimension and the target density have been chosen to be coherent with the potentiality of the PLD technique for producing metallic foams. The chosen thickness is enough to allows the full energy deposition. The value of the laser intensity is chosen consistently with the potential of the ABC facility. The numerical values of the parameters are shown in Table 5.3. In Figure 5.8 are shown the profiles of density, electron temperature, ion temperature and radiation temperature resulting from the irradiation of the gold foam after 0.4 ns, according to what is shown in [32].

Table 5.3: Gold foam target

EOS	thick[cm]	pore[μm]	av. ρ [g/cm^3]	Intensity [W/cm^2]
Gold as ideal gas	0.05	1	0.1	10^{14}

Table 5.3: Radiation on

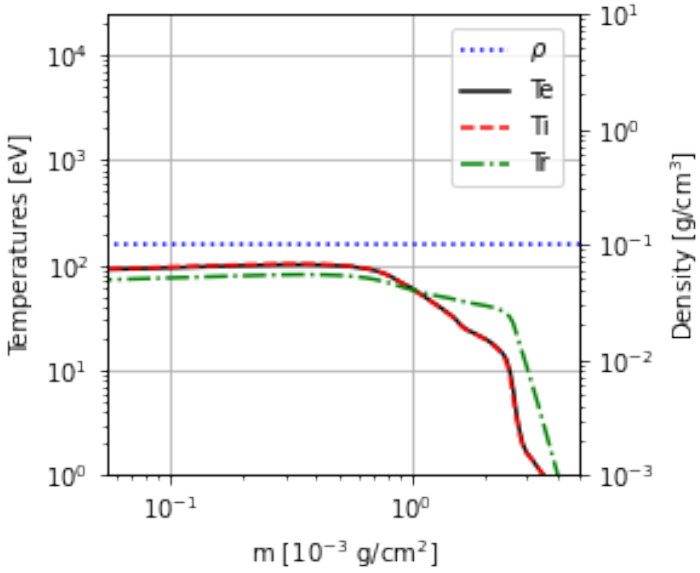

Figure 5.8: Gold foam target. Pore dimension 1 μm, ABC laser irradiation conditions.

As shown in figure 5.8 the density profile is completely flat, accordingly to what is observed in section 4.4. The shock formation zone seems to be suppressed to an higher extend

respect to the LDG case. This may allow me to say that the laser energy which is no longer involved into the shock formation is converted into X-rays. This would imply an even higher conversion efficiency of the laser energy into X-rays, with respect to the LDG case shown in [32]. Of course a dedicated experimental campaign is necessary since there are some aspects of the interaction which are not completely clear and some other phenomena may be involved.
Last but not least also in this case I want to conclude the target design taking into account for the production techniques, namely, ns-PLD or fs-PLD.Differently to the carbon, gold exhibits a liquid phase. Therefore the droplets formation due to the laser ablation is a serious problem since once deposited onto the substrate they will drive the aggregate toward a compact bulk film situation. The droplets formation is enhanced in the ns-PLD. On the other hand in the fs-PLD has been observed aggregation on-substrate aggregation mechanisms between micro-metric and nano-metric particles which may lead to a partial homogeneization of the aggregate. In this situation I may say that the lesser evil is to accept the on-substrate aggregation mechanism and go for a fs-PLD.

5.2.1. How to determine the radiative heat wave regime

The radiative heat wave corresponds to the radiative temperature profile which is evolving into the target due to the laser ablation. As we have seen in 4.4 our aim was to verify the propagation regime for the radiative heat wave. This can be done through the measurements of the propagation velocity of the plasma front on the rear side of the ablated target and of the radiative heat wave velocity. The propagation velocity of the plasma front as emitted by the surface will coincides with the shock velocity developed into the target. For what concerns the measure of the former we need an optical streak camera while for the latter a X-Ray streak camera is required. In both cases we can use the self-emitted light of the target. Optical and X-ray streak cameras work the same way. The difference is just related to the photocathode. In the optical case the photocathode needs to be sensitive to the photons having a wavelenght into the optical region ($390-700$ nm). The X-ray streak camera is sentitve to photons having a wave length in the range $0.1-10$ nm. The radiative regime is said to be *supersonic* if the radiative heat wave progates faster than the shock wave. Otherwise the radiative regime is said to be *subsonic*. In Figure 5.9 the experimental set-up has been presented.

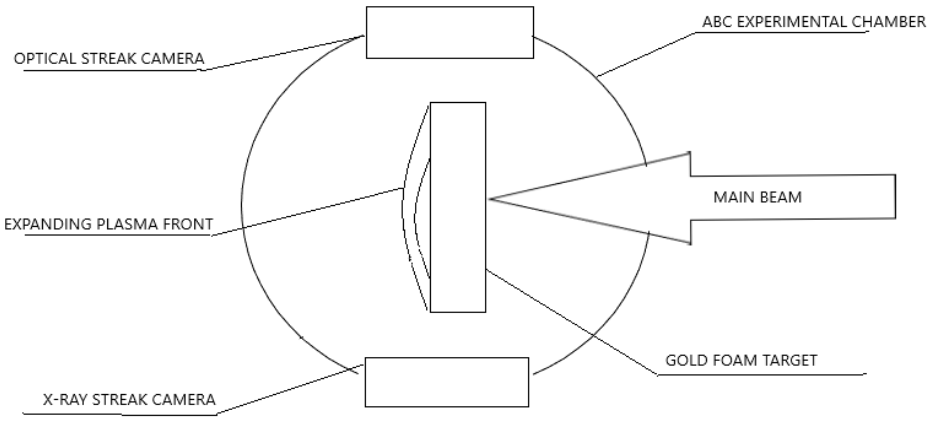

Figure 5.9: Experimental set-up for the radiative heat wave regime determination.

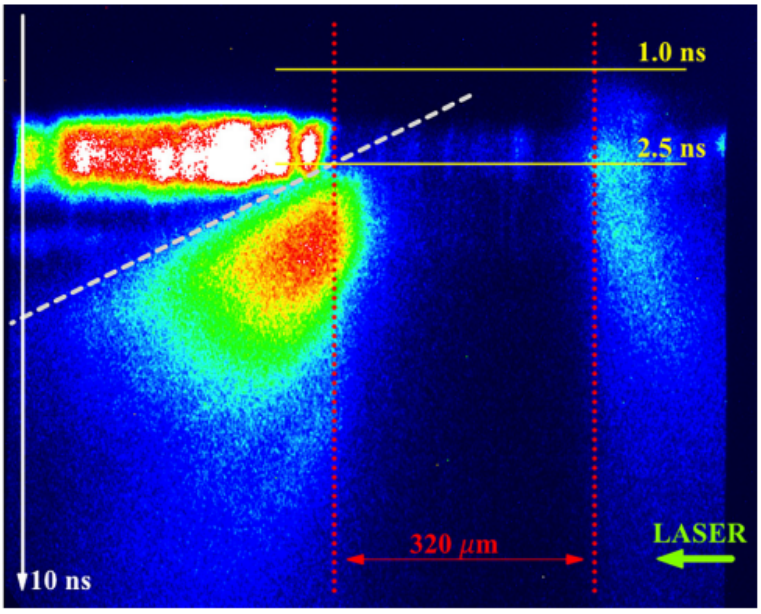

Figure 5.10: This is a shoot obtained by an optical streak camera, available from the ABC database.The streak acquisition time is 10 ns, while the target width is 320 μm (ENEA archive).

In Figure 5.10 the plasma on the laser side is visible after 1 ns from the shot time, while the plasma on the rear side is visible after 2.5 ns. The main laser beam is coming from the right. The white dashed line indicates the expansion velocity of the plasma produced on the back side of the target and is used to estimate the breakout time of the shock wave (ENEA archive). Through an X-ray streak camera we could measure the breakout time for the radiative heat wave. The comparison tells us which is the propagation regime.

6 | Conclusions and future developments

6.1. Conclusions

The work I carried out in my thesis has been entirely theoretics.
In chapter 1 I talked about the macroscopic environment of nuclear fusion science.
Starting from chapter 2 the focus was considerably reduced. I explained the state of the art concerning foam materials, ablators, and hohlraums for ICF, the differences and the analogies between, respectively, the PLD deposition regimes and fractal models. The section Aims of the work is devoted to explaining the main aspects I investigated.
In chapter 3 all the physics involved in the MULTI-FM 1D code has been explained. This chapter constitutes a good reference for learning both introductory aspects and advanced technicalities of the code.
In chapter 4 I performed simulations having the aim of explaining the physics involved in laser foams ablation experiments, for both carbon and gold. The chapter offers important explanations of the basic aspects of the interaction up to those related to the fractality of these foams.
Moving to the end, in chapter 5 I presented optimized designs for carbon foam target as ablator and gold foam target as hohlraum. For what concerns the former, since MULTI-FM 1D through the years has been continuously validated by experiments, I had the possibility of performing a deep analysis of the physics taking into account technical issues too. For what concerns the latter the MULTI-FM 1D code does not have a validation once the radiation field is active together with the foam model. This is the reason for showing a less accurate design. Nevertheless, the comparisons performed with the work presented in [32] are quite promising.
As I am going to show in the next sections, many open points are left that have to be seen as great opportunities for improving our understanding and realize more efficient and reliable devices for a green future.

6.2. Future developments: Upgrading MULTI-FM and future experiments at the ABC facility

In this section I am going to explain to which extend the results of my work can be improved. At end I will talk about the laser facilities which can be involved for the validation of the results.

6.2.1. Upgrading MULTI-FM

The MULTI-FM version at my disposal is a well validated one. Nevertheless in the next future I expect to partecipate to the develpment of the 2D version. For the sake of clarity a 2D version of MULTI-FM already exists but a 2D version of MULTI-FM which takes into account for the internal structure is lacking. This upgrade will give us the capability of simulating a number of hydrodynamical phenomena which cannot be simulated in the 1D version; turbolences and hydrodynamical instabilities such as the Rayleigh-Taylor are just an example. The lateral spread of the energy distribution would be taken into account too. This upgrade would give me the possibility of verifying what I supposed at the and the end of section 4.3 about the possibility of a moderation of the RT instability into foam materials. Quoting [14] the problem related to hydrodynamical instabilities is a serious one. It is more severe in the direct scheme respect to the indirect scheme, thanks to the black body radiation coming from the hohlraum. Unfortunately the use of an hohlraum and so of the indirect scheme do not implies a complete suppression of hydrodynamical instabilities. The use of a foam ablator in an indirect scheme may represent a new better solution. Moreover, a 1D code does not take into account for the lateral spread of energy during the laser ablation. This effect is expected to have two main conseguences. First of all we will observe a slow down of the homogenization process; this is on the side of increasing the pressure level since, as explained in [8], this slowing down would increase the energy available at the moment of the shock formation. The second effect is on the opposite side since a lateral spread of energy implies a bigger volume into which the laser energy can be accumulated; a lower pressure wavefront is expected. A competion between these effects will take place, which means that there will be again the possibility for a better optimization of the target having the aim to achieve even higher pressures. A parallel code for simulating parametric instabilities could be developed too. By parametric instabilities we refer to: Raman Scattering, Brilloin Scattering, Two Plasmon Decay. These phenomena are quite deletering for the laser energy conversion efficiency since basically a photon can undergo these phenomena instead of just being absorbed by the matter. A better understanding of how these instabilities into the foams is for sure a

crucial point for both ablator and hohlraum applications. Also from this point of view I do not found any article devoted to the analysis of the impact of parametric instabilities on a carbon foam ablator and a gold foam hohlraum. Experiments at the ABC facility may be carried out having the aim of validating my thesis work and my conclusions. In any case It will be a step forward in the comprehention of how foams interact with lasers. By recalling what I wrote in Sec.3.3 there will be the possibility to study how to improve the effective absorption model. Of course an intense experimental activities will be required. An absorption coefficient which varies depending on what happens when the laser light travels through the targert taking into account for the fractality of the foam too does not exist yet. The absorption model (Sec.3.3) which is implemented in MULTI-FM right now is an effective coefficient. The improvement absorption model must be obtained from reasoning based on first principles. This is another very interesting and stimulating open problem which I want to face in next future.

6.2.2. Fractal model comparison

As explained in section 2.5.2 there is an evident connection between the Gus'kov's fractal model and the fractal model developed by the NanoLab group. I explained how one should perform the experiments having the aim of demonstrating if the equation 2.6 I wrote is correct or not. This will be the first time for performing such a comparison. The ABC facility and the NanoLab group have all the required diagnostics for performing this kind of analysis. The importance of this equation is due to the fact that once validated one have a real instrument to control the fractal parameter α which appears in the Gus'kov's model. This parameters has always been experimentally determined without any possibility of really controlling it due to the foam production methods which has been used untill now [17, 22]. The influence of the fractal parameter on the hydrodynamics/heat transport/ radiative transport developed in a fuel pellet due to the interaction with a high intensity laser would represent a completely new subject since there no available studies about this problem.

6.2.3. EOS measurements

Last but not least let us remember what is written in 4.5 about the reason why I did not get exactly the same results which appear in [32]. This little discrepance in the results is mainly due to the EOS, which in the ICF field is maybe the most important aspect to deal with. Moreover, in literature there are no available EOS data concernings any kind of foam materials. For these reasons I will strongly promote the realization of experimental campaigns having the aim of measuring the EOS of the target produced by

the NanoLab. This can be done through the so called Velocity Interferometer System for Any Reflector (VISAR)(Appendix B). This diagnostic is currently in development at the ABC facility and I will actively partecipate to its completion, therefore in the next future such a measure could be performed, for both carbon and gold foam targets. VISAR uses interferometric techniques to measure the shock waves propagation velocity. Thanks to the information provided by the VISAR we can infer about the EOS ([14]). Once the code has been upgrated, the absorption model has been improved, EOS equations for the real targets has been determined I will reproduce all the significant simulations appearing in this thesis work having the aim of making a meaningfull comparison. Then, thanks to the experimental validation of them, a step forward in the comprehention of these novel materials and the way they interact with HIL will be possible.

6.2.4. Experimental roadmap

I plan to actively partecipate to the future develpments of this thesis work. I want to mention the fact that, during the period of my PHD, I will apply for laser time at facilities with competitive access such as ABC in Italy and VULCAN in UK. Performing experiments at different facilities would give me an high level validation of my work. At the ABC facilities there will be the possibility for performing the experiments on both cluster assembled carbon and gold foam target as explained, respectively, in Sections 5.1.1) and 5.2.1. At the VULCAN facility the VISAR is available. This will give me the opportunity of applying for laser time in order to perform experiments having the aim of obtaining the tabular EOS for cluster assembled foams produced by the NanoLab, in Politecnico di Milano. Both these campaigns once completed will result in an improvement of both the physical understanding of the laser foam interaction and the available database.

6.2.5. Foam applications outside the ICF context

I want to conclude mentioning that the nanostructured foams I have taken into account in my work (those produced by the NanoLab) were originally devoted to other applications,such as particle's sources [24] and particle's acceleration [23]. So, despite the fact the focus of the present work has been ICF a part of the conseguences derived from my analysis may be properly translated into other applications. I want to highlight the concept of "properly translated", since for the aforementioned applications the regimes of interest are very different from what is interesting in ICF. Orders of magnitude of difference between the laser intensities. This have strong conseguences on how matter react to the irradiation. Lasers involved into ICF have a few ns duration usually. This means that ions and electrons can both partecipate to the interaction; electrons being much lighter than ions

react much faster, but these durations allow for a fully developed ions dynamics. In fact MULTI-FM is two fluid code, since ions actively partecipate to the hydrodynamics development into the matter. The lasers commonly used for both particles acceleration and particles generation have durations of the order of fs, even hundreths of fs : $1ns = 10^{-9}s$ and $1fs = 10^{-15}s$. The time scales are completely different and so the phenomena occuring into the same foam are completely different. Nevertheless the approach used in this work can be extended down to these time durations by properly changing the numerical tool and understanding which phenomena becomes relevant.

Bibliography

[1] C. M. Atzeni S. Burn performace of fast ignited, tritium-poor icf fuels. Nuclear Fusion, 37:14, 1997.

[2] R. P. Drake. High-energy-density physics: Foundation of inertial fusion and experimental astrophysics. Springer, page 651, 2016.

[3] A. K. et al. Comparison of plastic, high density carbon, and beryllium as indirect drive nif ablators. Physics of Plasmas, 25:15, 2018.

[4] A. K. et al. Symmetric fielding of the largest diamond capsule implosions on the nif. Physics of Plasmas, 27:11, 2020.

[5] A. M. et al. High-density carbon ablator experiments on the national ignition facility. Physics of Plasmas, 21:12, 2014.

[6] B. R. et al. High-density and high -ρr fuel assembly for fast-ignition inertial confinement fusion. Physics of Plasmas, 12:N, 2005.

[7] C. G. et al. Local thermodynamic equilibrium in laser-induced breackdown spectroscopy: Beyond the mcwhirter criterion. Spectrochimica Acta Part B, 65:86–95, 2010.

[8] C. M. et al. Laser-supported hydrothermal wave in low-dense porous substance. Laser and Particle Beams, pages 121–128, 2018.

[9] C. M. et al. Laser-driven hydrothermal wave speed in low-z foam. Physics of Plasmas, 25:9, 2018.

[10] C. M. et al. Time-dependent measurements of high-power reflection by low-z foam plasma. High Power Laser Science and Engineering, 9:14, 2021.

[11] D. A. R. et al. Laser-ablated loading of solid through foams of overcritical density. Physics of plasmas, 22:8, 2015.

[12] D. R. et al. Hugoniot data of plastic foams obtained from laser-driven shocks. Physics Review, 73:4, 2006.

[13] D. Y. et al. Efficient soft x-ray sources from laser-irradiated gold foam targets with well-controlled impurities. Nuclear Fusion, 58:121–128, 2018.

[14] E. M. et al. Ignition on the national ignition facility: A path towards inertial fusion energy. Nuclear Fusion, 49:9, 2009.

[15] G. V. N. et al. National direct-drive program on omega and the national ignition facility. Plasma Physics, 59:9, 2017.

[16] K. M. et al. Equation of state data experiments for plastic foams using smoothed laser beams. Physics of Plasmas, 6:6, 1999.

[17] K. N. et al. Fabrication of aerogel capsule, bromine-doped capsule, and modified gold cone in modified target for the fast ignition realization experiment (firex) project. Nuclear Fusion, 49:10, 2009.

[18] M. et al. Review of progress in fast ignition. Physics of Plasmas, 12, 2005.

[19] M. A. et al. Growth dynamics of pulsed laser deposition nanofoams. Physical Review Materials, 3:9, 2019.

[20] M. A. et al. Production of carbon nanofoam by pulsed laser deposition on flexible substrates. Springer, 2022.

[21] M. A. et al. Pulsed laser deposition of carbon nanofoam. Elsevier, 599:55, 2022.

[22] N. B. et al. regular foams, loaded foams and capsule suspension in the foams for hohlraums in icf. Fusion Technology, 38:115, 2000.

[23] P. M. et al. Toward high-energy laser-driven ion beams: Nanostrctured double-layer targets. Physical Review Accelerators and Beams, 19:6, 2016.

[24] P. M. et al. Advanced laser-driven ion sources an their applications in materials and nuclear science. Plasma Physics and Controlled Fusion, 62:21, 2020.

[25] R. J. S. et al. Lead (pb) hohlraum: Target for the inertial fusion energy. Scientic Reports, N:4, 2013.

[26] R. O. N. et al. Interaction of relativistically intense laser pulses with long-scale near critical plasmas for optimization of laser based sources of mev electrons and gamma-rays. New Journal of Physics, 21:15, 2019.

[27] R. O. N. et al. High-current laser-driven beams of relativistic electrons for high energy density research. Plasma Physics, 62:15, 2020.

[28] R. R. et al. Mutli-a computer code for one-dimensional multigroup radiation hydrodynamics. Computer Physics Communications, 65:86–95, 2009.

[29] R. R. et al. Mutli-fs -a computer code for laser-plasma interaction in the femtosecond. Computer Physics Communications, 183:637–655, 2012.

[30] R. S. et al. Heterogeneous flow and brittle failure in shock compressed silicon. Journal of Applied Physics, 114:31, 2013.

[31] S. A. et al. Shock ignition of thermonuclear fuel: principles and modelling. Nuclear Fusion, 54:22, 2014.

[32] Y. D. et al. Detailed energy distributions in laser-produced plasmas of solid gold and foam gold planar targets. Physics of Plasmas, 20:6, 2013.

[33] J. W. Forbes. Shock wave compression of condensed matter. Springer, page 382, 2012.

[34] R. V. B. Gus'kov S Yu. Interaction of laser radiation with a porous medium and formation of a non-equilibrium plasma. Quantum Electronics, 27:696–701, 1997.

[35] L. E. M. Landau L. D. Fisica teorica. Editori Riuniti, 5:704, 2010.

[36] J. M.-T.-V. S Atzeni. Inertial fusion:beam plasma interaction, hydrodynamics, dense plasma physics. Oxford Science Publications, page 453, 2003.

[37] S. V.A. Ignition of a laser-fusion target by a focusing shock wave. Plasma Physics, 9:240, 1984.

A | Appendix A: Shock Physics

A.1. Shock waves

Why do nature decide to reacts through shock waves once properly sollecitated? Acoustic waves is the main mechanism occuring in ordinary matter responsible for mechanical energy transfer. Nevertheless under certain conditions matter reacts by means of shock waves. This happens when the applied stress would imply a transition to a material state characterized by density, temperature and pressure order of magnitude higher respect to undisturbed state. When the involved energy is simply too high a simple acoustic wave cannot transfer such an energy. A shock wave is a sudden transition in the properties of a medium, involving a difference in flow velocity across a narrow (ideally abrupt) transition. Such a phenomena is related to three effect:

- It carries energy forward at the shock velocity, which depends on the medium chacteristics;
- It heats and accelerate the medium as it passes, so that the fluid behind the shock carries kinetic energy and internal energy;
- The shock heats the medium behind its front, so that its motion relative to the heated medium is subsonic.

In order to modeling the shock we can idealize a discontinuos transition between the upstream and downstream quantities. Nevertheless mass, momentum and energy must be conserved. As I mentioned in 1.1 entropy is not conserved in a shock transition due to the generation of heat which is accumulated into the transition thickness. The preservation of conservation laws through a shock transition is what leads to the enstablishment of the so called Hugoniot's conditions.

- Mass conservation: $\frac{\partial \rho}{\partial t} = -\nabla \cdot (\rho \vec{u})$;
- Momentum conservation: $\frac{\partial (\rho \vec{u})}{\partial t} = -\nabla \cdot (\rho \vec{u} \vec{u}) - \nabla p$;
- Energy conservation: $\frac{\partial}{\partial t}\left(\frac{\rho u^2}{2} + \rho \epsilon\right) = -\nabla \cdot \left[\rho \vec{u}\left(\epsilon + \frac{u^2}{2} + p\vec{u}\right)\right]$.

Where ρ is the mass density,$\vec{u}$ is the fluid velocity, p is the pressure,ϵ is the internal energy. For the sake of simplicity let us assume to perform a 1D integration of the mass conservation equation:

$$\int_{x_1}^{x_2} \frac{\partial}{\partial t}\rho \, dx = \int_{x_1}^{x_2} \frac{\partial}{\partial x}(\rho u) \, dx \tag{A.1}$$

Applying the divergence theorem on the right hand side:

$$\int_{x_1}^{x_2} \frac{\partial}{\partial t}\rho \, dx = (\rho u)_{x_2} - (\rho u)_{x_1}. \tag{A.2}$$

As you can see the left hand side of the equation above approaches zero when $x_1 - x_2$ (which can be seen as the shock thickness) becomes infinitesimal. Therefore:

$$(\rho u)_{x_2} = (\rho u)_{x_1}. \tag{A.3}$$

Through a shock transition. This is the first Hugoniot's condition. The others can be obtained the same way recasting momentum conservation and energy conservation:

- $(\rho u)_{x_2} = (\rho u)_{x_1}$;
- $(\rho u^2 + p)_{x_2} = (\rho u^2 + p)_{x_1}$;
- $\left[\rho u \left(\epsilon + \frac{u^2}{2}\right) + pu\right]_{x_2} = \left[\rho u \left(\epsilon + \frac{u^2}{2}\right) + pu\right]_{x_1}$.

All the shock physics analytical apparaturs nowadays is based on these relations, Hugoniot's conditions, and on a proper modelization of the fluid (so a proper analytical modelization of the EOS). If we can assume ideal gas (As I have done in all the simulations carried out in chapter 4 for both carbon and gold foams) then a polytropic relation among the fluid parameters can be written. Looking at the Hugoniot conditions in fact we read 3 equations and 4 variables (density, fluid velocity, internal energy, pressure). An equation of state is then necessary in order to get usefull solutions.

$$\rho\epsilon = \frac{p}{\gamma - 1} \tag{A.4}$$

Is a possible way to recast the polytropic EOS for an ideal gas, as reported in [2]. However, for high-energy-density physics an additional complication arise since the polytropic index γ greatly changes across the shock transition. We can use the Hugoniot's conditions by properly adapting the value of gamma downstream and upstream.

A.2. Weak Shock limit

The weak shock limit is what can be described when one can assume $p_2 \to p_1$.

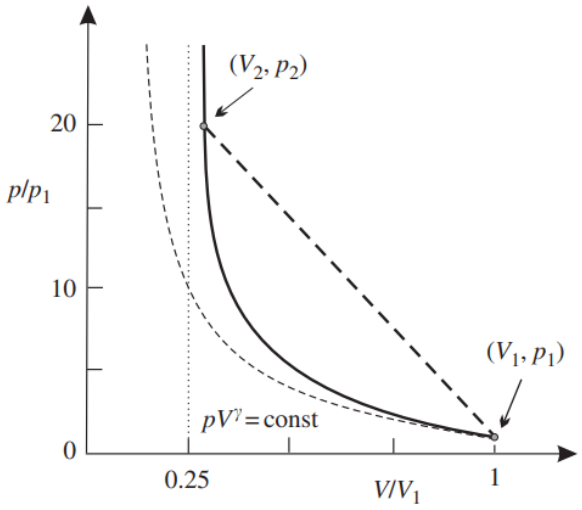

Figure A.1: Hugoniot adiabat (solid line) for an ideal gas having $\gamma = 5/3$ in the P-V plane. The thick dashed line is the so called Poisson adiabat ($PV^\gamma = const$) [36].

In this limit the energy downstream is enhanced just due to mechanical work. The amount of heat produced is, in this ideal limit, infinitesimal and therefore the entropy production too. This is of course an idealization of the real situation and for sure is not even close to what happens during the fuel pellet implosion.

A.3. Strong Shock limit

The strong shock limit is what can be described when one can assume $p_2 \gg p_1$. This is a very important point for the comprehention of which are the performances of a compression realized through a shock. The compression ratio p_2/p_1 of an ideal adiabatic compression can be infinite. Shock compression do not exhibits such a compression ratio. The upper limit of this ratio can be easily found by properly manipulat the hugoniot adiabat in the strong shock limit (assuming ideal gas model):

$$\left(\frac{p_1}{p_2}\right)_{\max} = \frac{\gamma + 1}{\gamma - 1} \tag{A.5}$$

Assuming $\gamma = 5/3$ (as it is assumed in my simulations concerning carbon) the compression ratio is equal to 4. So the pressure downstream cannot be higher than 4 times the pressure

upstream a shock (instant by instant). For the sake of clarity I am not saying that starting from a given pressure the final pressure cannot be higher then 4 times the initial pressure. This must be applied instant by instant to each shock profile during the propagation into the target.

A.4. Rarefaction waves

A rarefaction wave is a decrease in density and pressure caused by the expansion of the material. In experiments involving matter ablation by a laser we observe firstly observe a rarefaction wave due to the outward expansion of the plasma. The corresponding decrease in pressure propagates into the target at the sound speed, and is accompanied by an outward flow of material and a corresponding density decrease. Then we observe a compression wave which if the conditions are matched results in a shock wave. When a shock wave escapes from a target surface into a lower density region, the high pressure produced by the shock causes the material to accelerate forward.We have a release of the shocked material into an unperturbed region. In high energy density physics this phenomenon is called shock breakout and it is particurarly important once one want to describe the physics beyond the ablator of a fuel pellet.

A.5. Blast waves

A shock wave end in two ways. Once it reachs a lower density medium a rarefaction wave propagate backward into the shocked material and the shocked material is released into the unperturbed regione. The other way is related to the source of pressure. If this source ends (the laser ablation turns off or the shock wave is far away from the ablated surface) a rarefaction wave is allowed to propagate forward overtaking the shock. The latter phenomena is what is called blast wave. I am going to shock a picture taken by [2]:

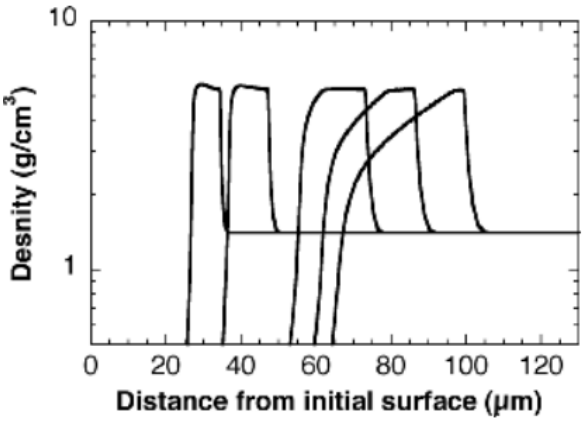

Figure A.2: This is a simulation of the evolution of a blast wave. Laser from the left to the right. This simulations has been performed by using a low density plastic target [2].

The reason why I am considering blast waves is that it has been shown [2] that they can be a souce for the Rayleigh-Taylor instabilities, at the separation surface between the ablator and the remaining part of the fuel pellet. This kind of instability is for sure deleterial for the compression efficiency of the fuel pellet.

B | Appendix B: Diagnostics

The ABC facility is one of the most equipped in the world. The potentiality for data analysis are quite impressive.In chapter five I showed the working principles of few diagnostics, just those important for explaining the concepts appearing in those sections. In this appendix I will briefily talk about other diagnostics that will be relevant once and experimental campaign at the ABC facility is performed.

B.1. Velocity Interferometer For Any Reflector (VISAR) for EOS measurements

Velocity Interferometer System for Any Reflector (VISAR) is a device whose working principle is very similar to that of the much more common Fabry-Perot interferometer, but the VISAR employs the relativistic Doppler shift. This diagnostic makes uses of very sofisticated interfermeter techniques by parallely performing comparisons with a very well characterized materials, whose EOS is already well known. Quartz is an example of material which can be employed for this kind of measure. It allow us to measure surface velocities of rapidly moving parts. This can be done by measuring the change in Doppler shift of light reflected off a moving surface.

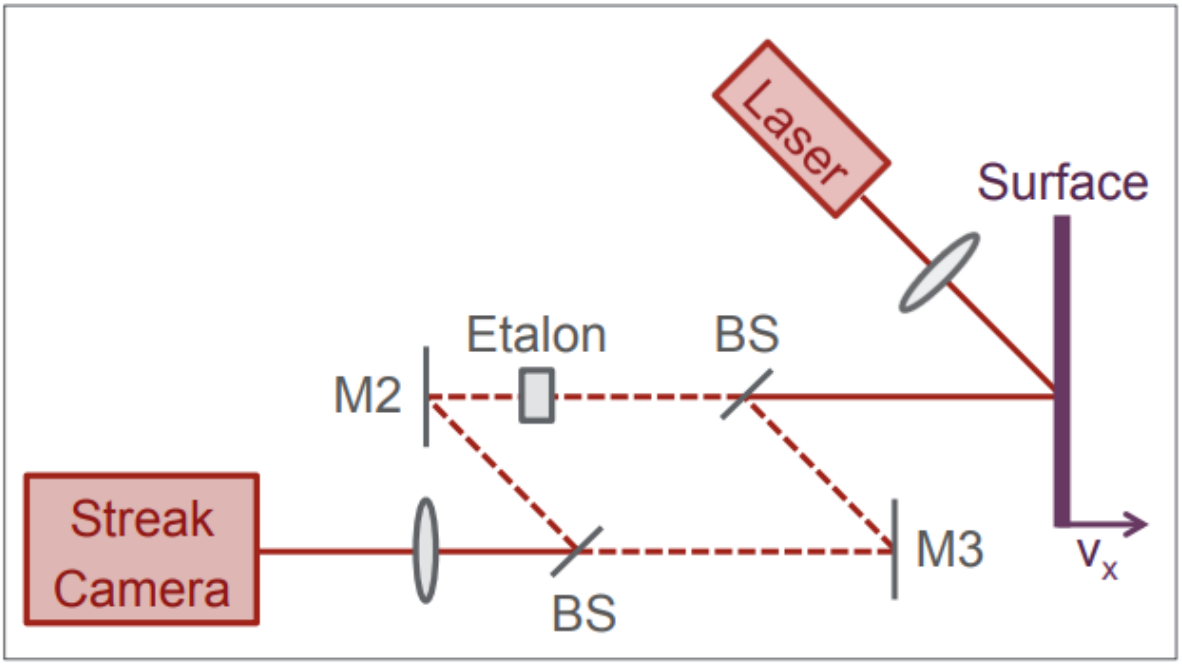

Figure B.1: Schematic representation of the VISAR set-up [30].

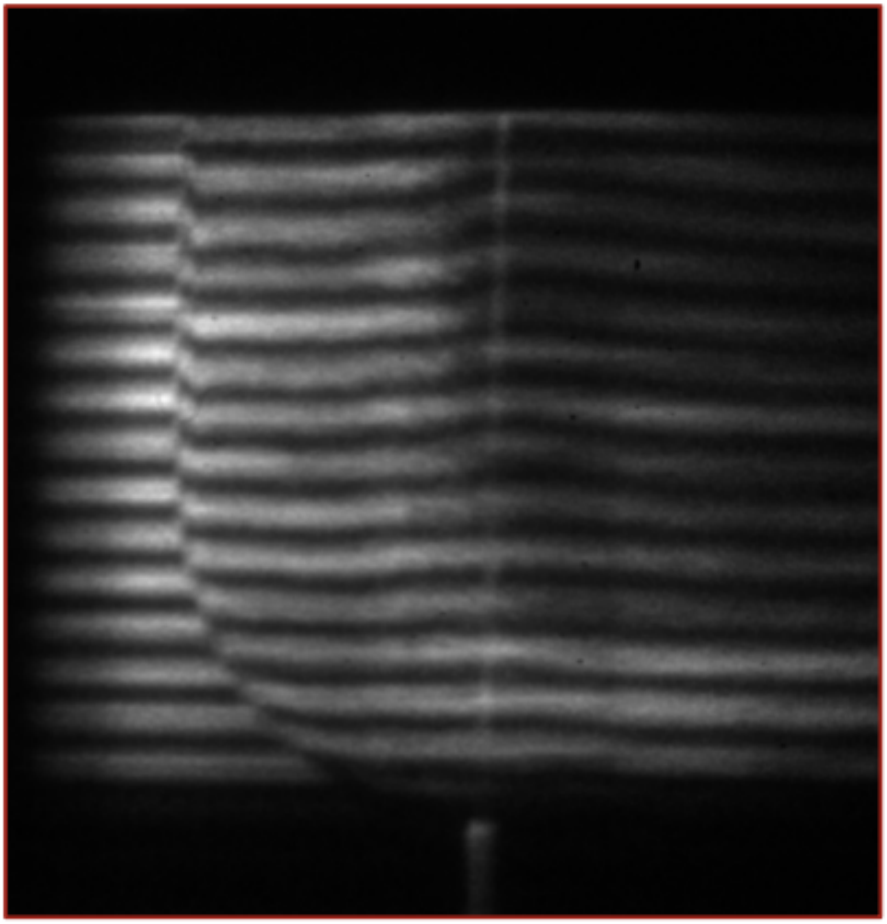

Figure B.2: Fringes pattern of the ablated moving surface [30].

The aim is to get the fringe phase through the evaluation of the Doppler shift. Once the fringe phase is evaluated the velocity of the moving surface can be connected to it [30]. So the experiments is performed in two main steps. First, by considering the reference material we know that since its EOS and its Hugoniot adiabat are very well characterized then by evaluating through the VISAR the shock velocity we can reconstruct the theromodynamic state of the reference material. Moreover, once the shock reach the end of the reference material layer it is reflected due to the higher density of the second layer. This reflection gives rise to a rarefaction wave propagating backward into the shocked reference material. Second, you ablate the target material you are interested in knowing the EOS and then you measure the velocity of the shock wave. By comparing the shock velocity of the latter and the rarefaction velocity of the former, into the plane in which the hugoniot of the reference material is plotted, you can get information about the pressure level of the material you are interested in. To get a point of the desired EOS you have to perform, under the same conditions, a measure of the plasma temperature at

the shock breakout (a Streak Optical Pyrometry can be used).

B.2. Streak Camera

In a steak camera the time profile of a pulse is transformed to spatial profile. We basically have a photocathode characterized by a work function. This work function is what makes the very important difference in between an optical streak camera and a X-ray streak camera.

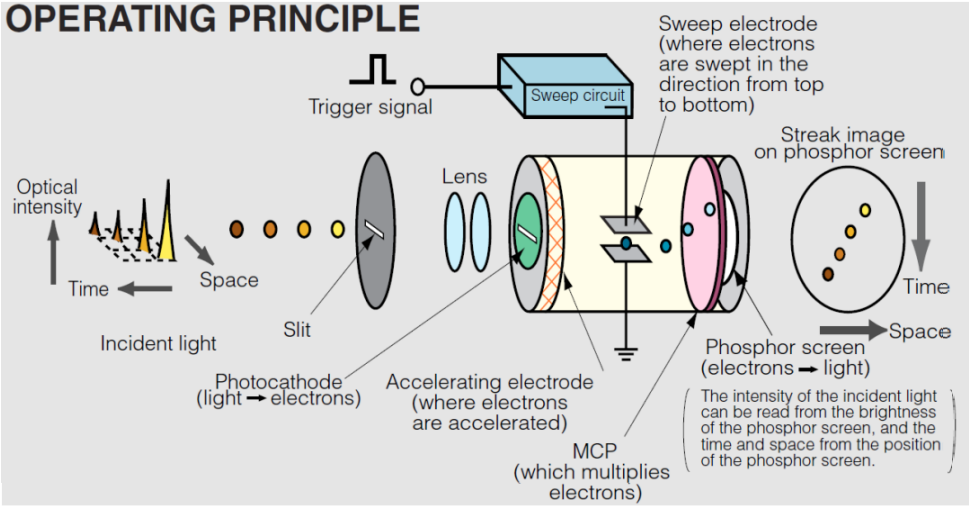

Figure B.3: This is the scheme of a streak camera (ENEA archive).

The slit dimension can be related to the temporal resolution of the streak camera. The tighter the slit the better the temporal resolution. Of course there is a downside. When the light signal of interest is weak you have to find a compromise between the capability of the streak of detecting the signal and the temporal resolution.

List of Figures

List of Tables

Acknowledgements

First I want to thank professor Matteo Passoni who gave me the opportunity to start this new collaboration with the Centro Ricerche ENEA through my thesis. From this point of view a general thanks goes to the Politecnico di Milano and the ENEA that, as istitutions, have represented a solid base during my formation. Last but not least I want to thank my family. There are no proper words to explain how big their contribution has been.